

## Conceptual Design Report of A Firefighting Very-Large-Air Tanker “Material Girl”



Submitted to the 2021-2022 AIAA Aircraft Designing Competition for Undergraduate Students

*University of Virginia*

*Department of Mechanical and Aerospace Engineering*

Team name: Hoos on Fire

Jemma Johnson

Jaylon Williams

Lama Khraibani

Logan Honts

Nicholas Martin

Quang Lam




Ryan Keough

Yicong Fu

Advised by: Dr. Jesse Quinlan

May 11<sup>th</sup>, 2022

## Team Information and Signatures

<p>Jesse Quinlan jrj2a@virginia.edu Faculty Project Advisor AIAA #: 306245</p>	<p>Jemma Johnson jj3df@virginia.edu Team Lead Propulsion Systems AIAA #: 1356959</p> 	<p>Jaylon Williams jw6ej@virginia.edu Design requirement Auxiliary analysis AIAA #: 1315244</p> 
<p>Lama Khraibani lak2db@virginia.edu FAA Regulations Propulsion System AIAA #: 1315245</p> 	<p>Logan Honts lph6cy@virginia.edu Structural Design, Aerodynamics, Stability &amp; Control, Payload AIAA #: 1325935</p> 	<p>Nicholas Martin nam3cs@virginia.edu Empennage design Aerodynamics AIAA #: 1357166</p> 
<p>Quang Lam qnl8ey@virginia.edu Autonomous Tech Cost analysis AIAA #: 1357164</p> 	<p>Ryan Keough rjk3pm@virginia.edu Digital Structures, Payload Fuselage and Anti-Icing Lead AIAA #: 1357165</p> 	<p>Yicong Fu yf5bp@virginia.edu Mission performance analysis Wing aerodynamics and aeroelastics AIAA #: 1356932</p> 

## Table of Contents

Team Information and Signatures	2
Table of Contents	3
List of Tables	5
Introduction	6
1. RFP	7
2. SOA	8
2.1 Introduction	8
2.2 Business/Operations	8
2.3 Aerodynamics	9
2.4 Structures	9
2.5 Propulsion	10
2.6 Anti-Icing	10
2.7 Autonomy	11
2.8 14 CFR Part 25	11
2.9 Cost	11
3. Final Design	12
3.1 Design Evolution	12
3.2 Final Design	13
4. Takeoff Gross Weight (TOGW)	15
4.1 Mission Profile	15
4.2 Estimation method	18
4.3 Estimation results	19
5. Matching Plots	25
5.1 Requirements and Constraints	25
5.2 Justification for input values	26
5.3 Results Explanation	27
6. Wings	28
6.1 Design Overview	28
6.2 Design Approach	29
6.3 Wing position	31
6.4 Fundamental wing geometric configurations	32
6.5 Airfoil selection	39
6.6 Aerodynamic surfaces	42

6.7 Maneuvers	44
6.8 FEA modeling	45
6.9 Summary	51
7. Empennage	53
7.1 Design overview	53
7.2 Empennage Shape and Sizing	54
8. Fuselage	58
8.1 Design overview	58
8.2 Design approach	58
8.3 General dimensions	59
8.4 Structural rigidity analysis	60
8.5 Payload Dropping Systems	60
9. Propulsion	63
9.1 Design overview	63
9.2 Design approach	64
10. Avionics, Technology, and Subsystems (Auxiliary Systems)	66
10.1 Flight Controls	66
10.2 Subsystems	66
10.3 Electrical System	67
11. Performance Analysis	68
11.1 Takeoff & Landing	68
11.2 Cruise	68
11.3 Range & Endurance	69
11.4 Stability and Control	70
11.5 Longitudinal Static Stability	70
11.6 Lateral and Directional Static Stability	72
11.7 Dynamic Stability	73
11.8 CG and Static Margin	74
12. Cost Analysis	78
12.1 Stakeholders	78
12.2 Cost analysis of the final design	78
13. Next Steps	79
14. Conclusion	83
References	84



## List of Tables

Table 1-1 Requirements and Objectives Compliance -----	7
Table 3-1 Call-out Identification From the Isometric View of the Final Design -----	13
Table 4-1 Mission Schedules Defined for FLOPS Input -----	19
Table 4-2 FLOPS Estimated Segment Fuel Weight Fraction -----	23
Table 4-3 Auxiliary Mission Summary Information -----	24
Table 5-1 Constraint Calculation Chart -----	27
Table 6-1 Wing Parameters -----	29
Table 6-2 Wing Version Comparison -----	31
Table 6-3 Wing Position -----	32
Table 6-4 Comparator Aircraft for Wing Sweep -----	35
Table 6-5 Comparison of Airfoil Types -----	39
Table 6-6 Comparison of Airfoil Geometries -----	40
Table 7-1 Empennage Shape Trade Study -----	51
Table 7-2 Vertical Stabilizer Details -----	53
Table 7-3 Tail Volume Coefficients of Comparator Firefighting Aircraft -----	53
Table 7-4 Trade Studies on Horizontal Tail Incidence Angle -----	54
Table 7-5 Tail Volume Coefficients of Comparator Firefighting Aircraft -----	55
Table 7-6 Horizontal Stabilizer Details -----	55
Table 9-1 Engine Characteristics -----	62
Table 11-1 Longitudinal Stability Characteristics -----	70
Table 11-2 Lateral and Directional Stability Derivatives -----	72
Table 11-3 Dynamic Stability Derivatives -----	74
Table 11-4 CG Location During Design and Ferry Mission -----	76
Table 11-5 Neutral Point and CG Location -----	77

## Introduction

Since 1950, the average global temperature has increased by over 0.75 °C (The Learning Network, 2020). Impacts of this planetary warming are seen in record-setting heat waves, worsening thunderstorms, and droughts, all of which are fuel for wildfires. Between 1984 and 2020, approximately six million acres of area were burned by wildfires in the United States of America alone. This insurgency demands government agencies to funnel more of their annual budgets into firefighting. Since 2005, wildfire and firefighting spending in California has more than tripled and as of 2020, has surpassed three billion dollars (Beam, 2021). As wildfires grow more expensive and uncontrollable, firefighting organizations face more pressure to keep their communities safe from the flames. Their solution to this problem: combat wildfires from all directions by utilizing aerial firefighting.

Responding to the increasing wildfires that occur as a result of planetary warming and climate change, the American Institute of Aeronautics and Astronautics (AIAA) created their competition to design a responsive aerial firefighting aircraft. The aircraft must meet a series of design requirements and objectives outlined in the competition Request for Proposal (RFP). The final deliverable is a technical report detailing a fully designed concept aircraft along with justifications for design choices.

Hoos on Fire, a team of eight undergraduate engineering students at the University of Virginia Department of Mechanical and Aerospace Engineering, working under the supervision of Professor Jesse Quinlan, developed the aerial firefighting aircraft dubbed “Material Girl”. Material Girl is a large, fixed wing aircraft designed specifically for aerial firefighting that uses Phos-Chek as a flame retardant. Besides the requirements and objectives given by the AIAA, the primary design drivers were maximum takeoff weight (MTOW), fuel efficiency, control and maneuverability, and customizable flame retardant deployment. The following sections outline the design process for and key characteristics of Material Girl, demonstrating its status as a potential future leader in aerial firefighting technology within the fleets of existing aircraft.

## 1. RFP

Material Girl was designed to satisfy all RFP requirements. To increase the competitiveness and effectiveness, payload capacity and full-payload design radius were designed to meet the objectives. This consideration is to augment the fire suppressing practicality and responsibility by introducing Material Girl to the very-large-airtanker (VLAT) fleet. Table 1-1 below lists the requirements and objectives on the left, whereas the right displays information on how the requirement or objective is met or where to locate justification.

**Table 1-1. Requirements and Objectives Compliance**

Requirement [R] or Objective [O]	Achievement	
[R] Entry into Service in 2030	Designed with existing materials, engines, and subsystems	✓
[R] Use of existing engines or one that will be in service by 2028	Rolls-Royce RB211-535	✓
[R] Assumptions on at least specific fuel consumption/efficiency, thrust/power, and weight must be documented	Detailed in following sections	✓
[R] 4,000 gal or [O] 8,000 gal fire retardant capacity	Designed to carry up to 8,000 gallons of payload	✓
[R] Multidrop capable	Designed for two 4,000-gallon drops	✓
[R] Fire retardant reload $\geq$ 500 gal/min	See Fuselage: Payload Deployment System	✓
[R] Retardant density of at least 9 lbs/gal	Phos Chek LC95	✓
[R] $\leq$ 150 kts or [O] $\leq$ 125 kts drop speed	Stall speed of 115 knots, drop speed at 150 kts	✓
[R] Drop altitude $\leq$ 300 ft	300 ft	✓
[R] 200 n mi or [O] 400 n mi full payload radius	400 n mi	✓
[R] 2,000 n mi or [O] 3,000 n mi design ferry range	2,000 n mi	✓
[R] 300 kts or [O] 400 kts dash speed	300 kts	✓
[R] $\leq$ 8,000 ft or [O] $\leq$ 5,000 ft at 5,000 ft MSL elevation on a +35°F day balanced field length	4682 ft	✓
[R] Capable of VFR and IFR flight with an autopilot	See 11.2 Subsystems	✓
[R] Capable of flight in known icing conditions	Electrothermal anti-icing (See SOA)	✓
[R] Meets applicable FAA 14 CFR Part 25 rules	See SOA	✓
[O] Autonomous operations systems and architecture	See SOA	✓

## **2. SOA**

### **2.1 Introduction**

The state-of-the-art (SOA) reports are subtopics that each focus on an area that is essential to designing an aircraft. These SOA studies provided us with up-to-date knowledge about the status quo of firefighting aircraft as a baseline for our design. Each member of Hoos on Fire took responsibility for an SOA subtopic to research on the available platforms and technologies as well as drawbacks and room for improvement. Information on all of the subtopics were gathered and utilized in order to help design the most effective and RFP-compatible aircraft.

### **2.2 Business/Operations**

Engineering skills are very important when designing an aircraft, but they are not the only ones needed. These designs need to be funded and have a business aspect, or the design will never leave paper. The market value for an aerial firefighting aircraft is between eight and nine billion dollars, and helicopters are often used to supplement the capabilities of fixed wing firefighting aircraft fleets. There are two main organizations that use these technologies in order to provide aerial firefighting services: the California Department of Forestry and Fire Protection and the US Forest Service/Department of Agriculture. However, these organizations are very broad and there is no specific wildfire prevention agency which results in fragmented operations. States are left to decide on strategy on their own which leads to confusion and asset overlap with most states opting to use helicopters out of convenience. As wildfires worsen due to global climate change, the demand for this technology is increasing.

We were tasked with designing a fixed-wing aircraft, in contrast to a helicopter. Even with this requirement, there are a lot of possibilities to choose from. Groups could design a single engine air tanker, large air tanker, very large air tanker, scooper, or tactical aircraft – depending on the rest of the requirements that had to be fit as well. The large payload volume required to be carried by the aircraft confined the aircraft parameters for firefighting application. While there are many options currently, such as other air tankers, we had to meet the requirements in the RFP and design a technologically capable aircraft to be deployed in 2030.

## **2.3 Aerodynamics**

One of the major design goals of this project is for it to be as aerodynamic as possible. When making the design decisions to improve aerodynamic capabilities, it is important to remember that three major components of the aircraft have an impact on this analysis: wings, vertical tail, and fuselage. For example, the airfoil chosen is going to have an impact on the total lift that the wing generates, and the way that the fuselage is designed with the nose and tail will impact airflow during flight as well.

In order to optimize aerodynamic capabilities, it is necessary to not only look at the components of the aircraft but also look at new technologies that can be added to aid in this requirement. Some examples include Co-Flow Jet airfoils (delays stall condition) and pulsed-jet actuators. These additions truly help achieve a better aircraft performance overall by providing an improved lift-to-drag ratio which allows for higher speeds. All of these capabilities can be tested on different flight softwares and wind tunnel experiments.

## **2.4 Structures**

The structure of the aircraft is very important as its size and design affects its aerodynamic capabilities. Each component is unique in its own way and provides its own purpose on the aircraft. The fuselage houses the payload and is the central connection structure; the wing generates lift and provides control; empennage provides aerodynamic support and control; landing gear absorbs landing loads and gives ground control. Other structures that impact the aircraft include engine placement and material selection. The placement of the engine is important as it impacts aerodynamic performance, the center of gravity, and could add maintenance complications. The materials chosen are also of importance because they affect the strength, longevity, and cost of the structure. All of these components combined have to be designed and sized properly in order to ensure a high-fidelity plane.

Based on the SOA structures research, it is recommended to switch from heavy, wire-braced structures to lighter, semi-monocoque forms over time. Aerospace-grade metal alloys and composites allow for rigid, yet lightweight aircraft structures. More complex design missions require complex geometries for landing gear and engine mount structures that vary on a case-by-case basis. Creating redundant designs that minimize the risk of fast fracture due to cyclic loading is important when designing long lasting aircraft. In the harsh environments around wildfires, temperature effects such as creep and expansion as well as corrosion become important contributing factors. Testing and routine inspection is paramount to ensure safety from these unexpected sources of failure.

## **2.5 Propulsion**

When it comes to the tradeoffs that are listed in the design requirements, turboprop and turbofan propulsion systems are the most relevant. Turboprops are for smaller and slower aircraft while turbofans are for larger and faster aircraft. In order to predict the performance of the chosen engine, the Brayton cycle was used as well as component-by-component modeling. Afterwards, a modern cycle analysis was done with GasTurb and Gas Turbine Simulation Program (GSP). A double annular combustor (DAC) was utilized to improve performance and additive manufacturing (AM) can create complex geometries that are not possible with traditional manufacturing techniques – in the event that the chosen engine/design requires extra steps.

## **2.6 Anti-Icing**

Icing is a major issue that many aircraft deal with, especially in colder climates. It occurs between 0 and -20 degrees celsius due to supercooled water droplets. Aircraft icing is when droplets in cool air freeze on leading surfaces such as the leading edge of a wing or antennae. There are three types of icing. Clear icing is the most dangerous form as it is the heaviest, transparent, smooth, and occurs at warmer temperatures. Rime icing is when small droplets freeze instantly and is rougher. Mixed icing accumulates quicker but it is white and semi-crystalline. The presence of this ice on aircraft surfaces disrupts the airflow around the aircraft, limits aircraft performance, increases weight and reduces lift on the wings, increases drag and reduces thrust on the propeller, increases the stall speed and decreases the stall angle of attack, reduces visibility, and blocks airflow to the engine.

The solution to this is to use anti-icing measures in order to prevent any issues as much as possible. By avoiding icing, pre-flight will be completed at a quicker rate and it will help prevent early stalls in the aircraft. If there is ice built up on a wing, it will stall earlier when entering a fire zone. This still is unrecoverable at “low and slow” mission standards, which is dangerous for a firefighting mission. The selection for the anti-icing system that should be used on firefighting aircraft is a hydrophobic airframe coating with an internal electrothermal system. This is because this selection prevents pre-flight and in-flight icing, is easy to maintain, is state-of-the-art and durable, and has nominal engine efficiency losses. The only downside is that it is expensive to install electrothermal wiring and actuators but it may be worth it to pay that upfront cost to prevent maintenance issues in the future.

## **2.7 Autonomy**

Autonomous aircraft technology has become a very big part of the aviation industry. Development in autopilot for unmanned aircraft and autonomous systems give the potential for nearly automated flight from takeoff to landing. This type of technology would allow the aircraft to have autopilot capabilities, be able to complete low visibility takeoff, and autoland. These features are essential when flying in smoky conditions and nighttime, both common conditions for wildfires. Other technologies that could also be included are automated detection of fire through imagery and obstacle avoidance through environmental detection as they already exist in other fields. Adding this technology to aerial firefighting aircraft is going to eventually be a huge step forward for the field.

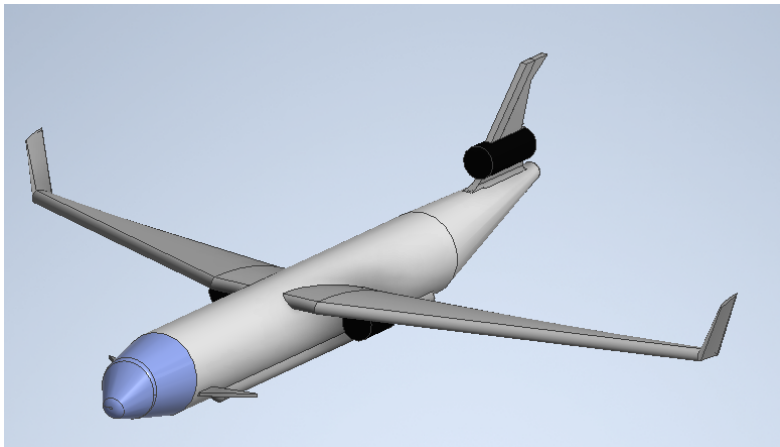
## **2.8 14 CFR Part 25**

When designing the aircraft, it is important to make sure that it adheres to the FAA regulations in 14 CFR Part 25. These regulations are divided into three main categories: takeoff/landing requirements, size/loading requirements, and reserve fuel requirements. The takeoff/landing requirements are to address high risk scenarios, size/loading requirements address structural needs, and reserve fuel requirements address emergency response capabilities. In order for the aircraft to be finalized and approved, it has to check off all of the corresponding requirements.

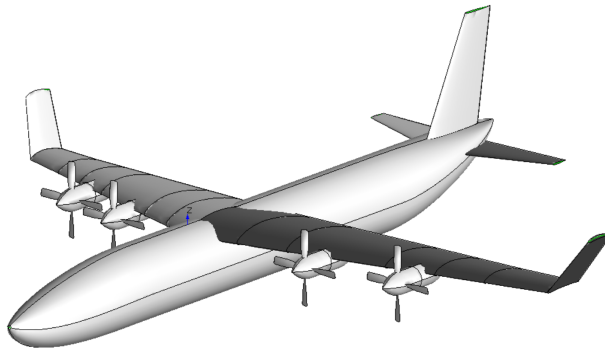
### 3. Final Design

#### 3.1 Design Evolution

Material Girl underwent two major design changes, creating three individual iterations seen below. These iterations were influenced by a series of repeated analyses using a variety of aircraft design programs. The first iteration of CAD modeling was done in SolidWorks to capture the general outline of the aircraft (Figure 3-1). It had three engines, like the DC-10, with two under the wing and one embedded in the vertical stabilizer. It had canards in lieu of the conventional horizontal stabilizers. After evaluating the necessity for certain technologies and features, the second iteration shown in Figure 3-2 converged more to the conventional air tanker design. It had a conventional cruciform tail and four under-wing turboprop engines. The shape of the cockpit was also modified to improve the aerodynamic performance.



**Fig. 3-1.** Material Girl 1: first design iteration

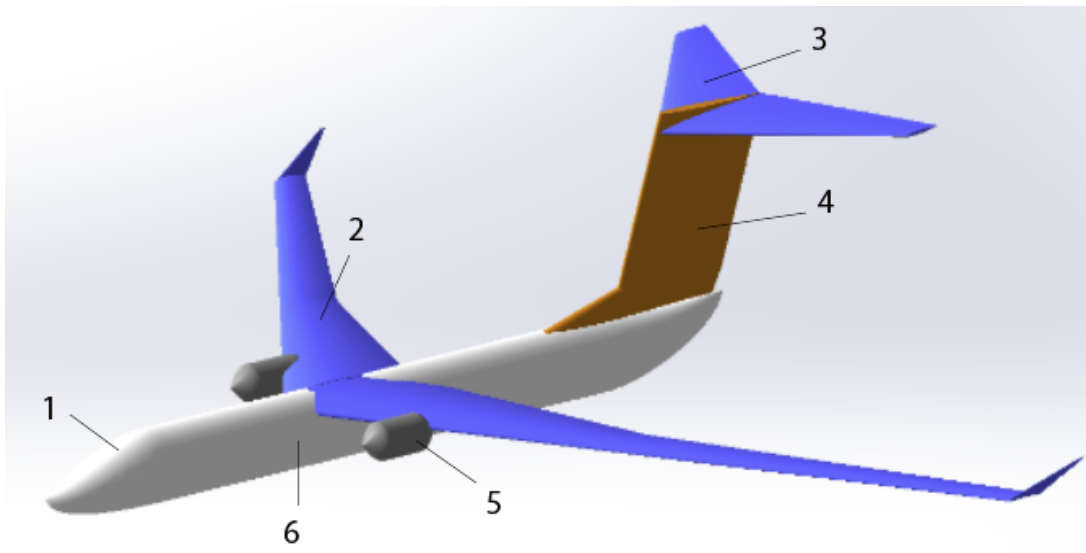


**Fig. 3-2.** Material Girl 2: second design iteration



### 3.2 Final Design

The final design was achieved after intensive multidisciplinary analysis and optimizations as presented in Figure 3-3 & 3-4. We are convinced that the final concept is able to provide a minimal fuel consumption, a minimal maximum takeoff gross weight, and a well-balanced firefighting mission performance. Details will be presented and discussed in the following sections.

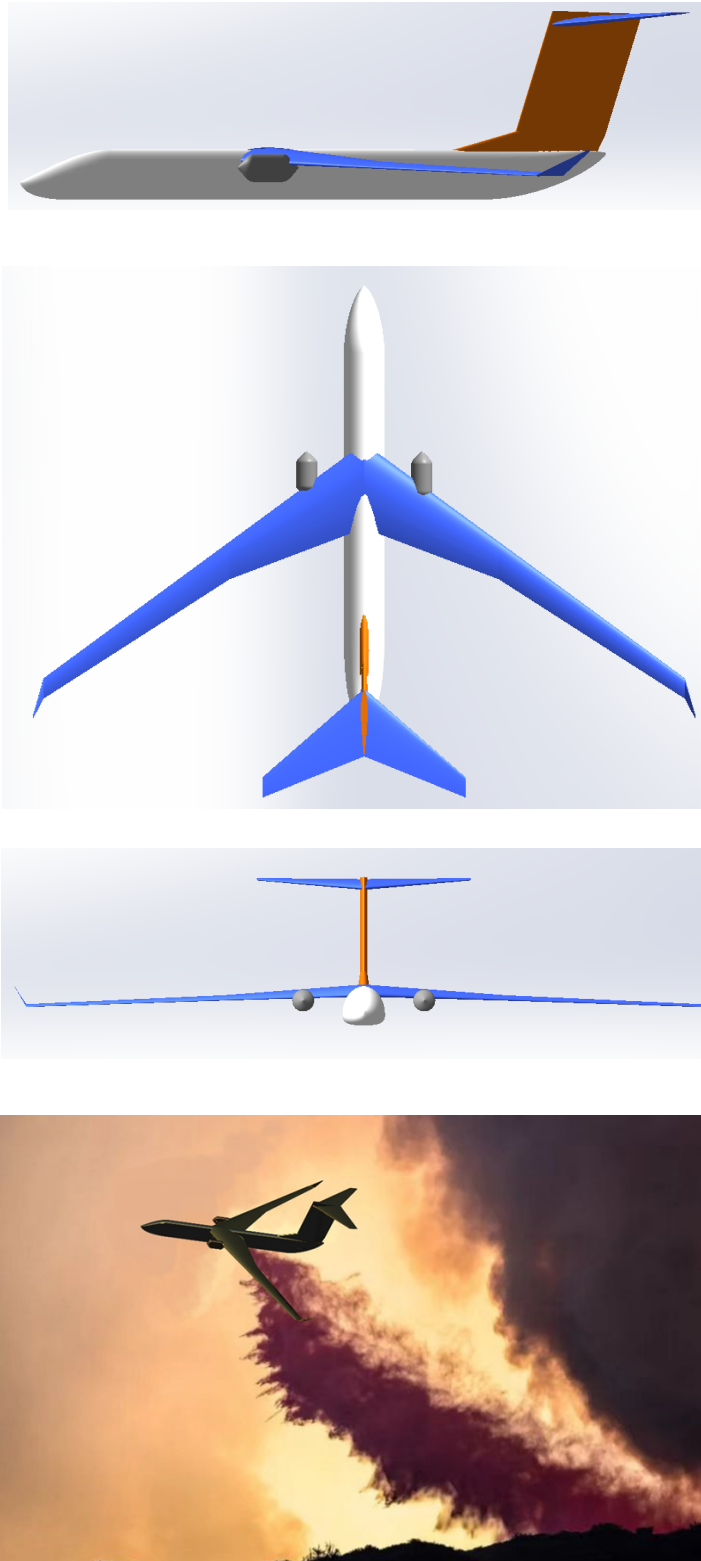


**Fig. 3-3.** Isometric view and feature call-outs of the final design.

Some characteristic features and modifications from the previous two iterations are summarized in Table 3-1.

**Table 3-1** Call-out Identification From the Isometric View of the Final Design

Key characteristics	
1	Contoured cockpit for good visibility
2	High-mounted, anhedral, ultra-high AR, swept, and high-cambered wing. High lift surfaced including flaps.
3	T-tail configuration
4	Large rudder for effective yaw and roll stability control
5	Two turbofan engines for ample trust and ground clearance
6	Flat-bottom fuselage for deployment and filling

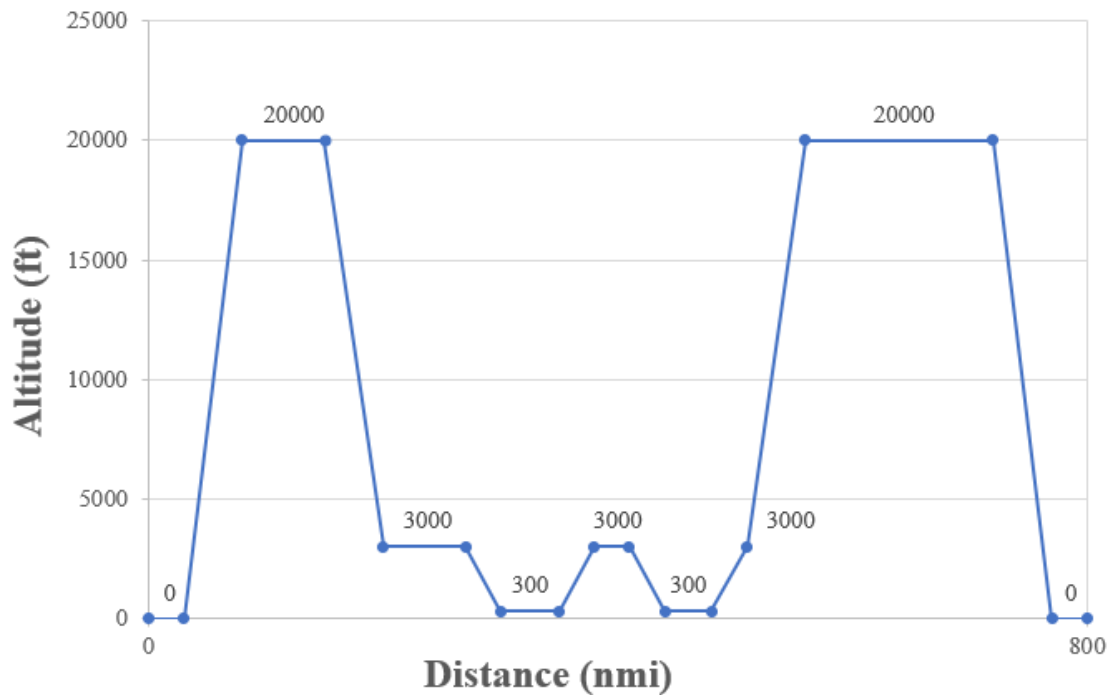


**Fig. 3-4.** Three-view drawings and rendered dropping maneuver.

## 4. Takeoff Gross Weight (TOGW)

### 4.1 Mission Profile

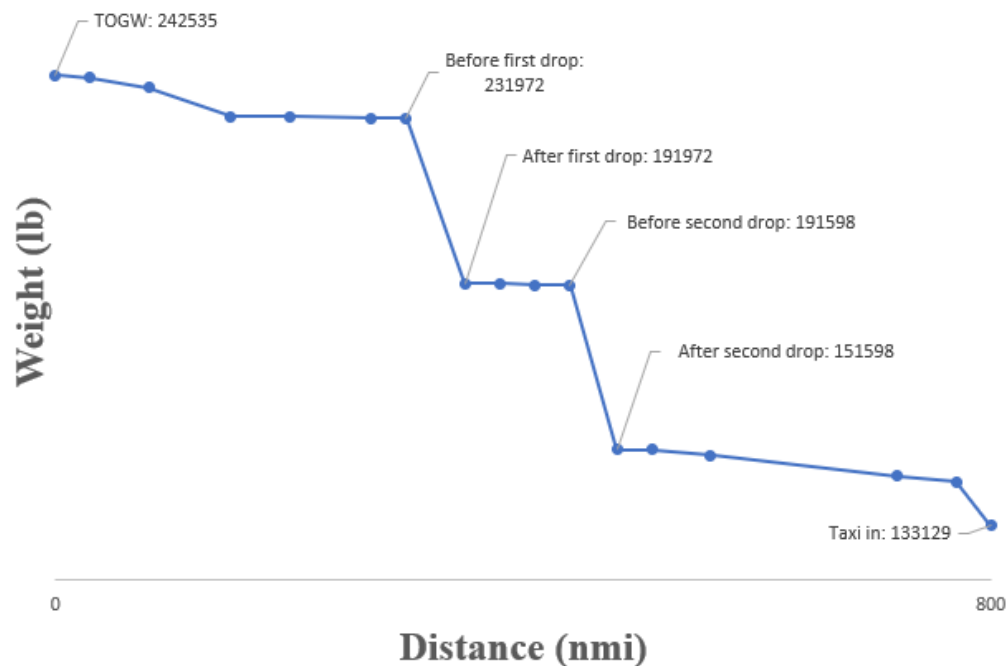
To understand the operations of our aircraft in a fire fighting mission, it is helpful to refer to the mission profiles depicting both altitude and weight information as a function of the flight distance (Figure 4-1). The visualizations would assist with understanding of the specific segments and their corresponding quantitative status.



**Fig. 4-1.** Altitude mission profile for full-payload firefighting.

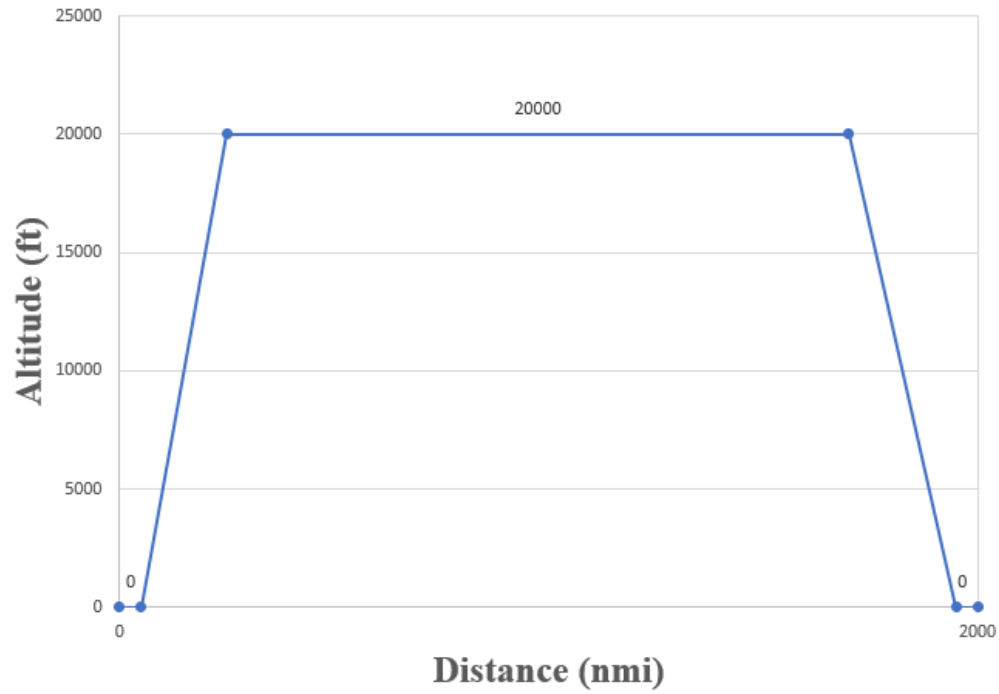
As shown above, our aircraft is nominally designed to achieve two retardant drops within a mission radius of 400 nmi, or a total mission range of 800 nmi. If visualized chronologically, the mission starts with taxi out and takeoff from the base airport, followed by a standard constant-rate climb to the cruising altitude at 20,000 ft heading towards the fire site, then enters a descent to 3,000 ft level as it approaches the fire site and prepares for dropping, then further descends to 300 ft to drop the first 4,000 gallons of retardant, then makes a quick dash back to 3,000 ft towards the second dropping site where it makes another descent to the 300 ft level to drop the other 4,000 gallons of payload, then makes another quick dash to 3,000 ft to be clear from ground objects and terrains, continued by a return flight with the same climb and cruise schedules, and finally descends back to the base airport for the next mission.

A weight profile was also made to depict the multi-drop capability of our aircraft by showing two separate retardant deployment schedules during the mission (Figure 4-2). Each time will have 40,000 lbs of retardant dropped directly onto or in front of the fire line to extinguish or prevent spreading. Assuming a density of 10 lbs per gallon, 40,000 lbs of payload will be equivalent to 4,000 gallons of fire retardant. Two drops will sum up to a total of 8,000 gallons of capacity, which meets the objective of the RFP, making our design very competitive for its large to very large airtanker (LAT/VLAT) capability expected in the firefighting fleet.

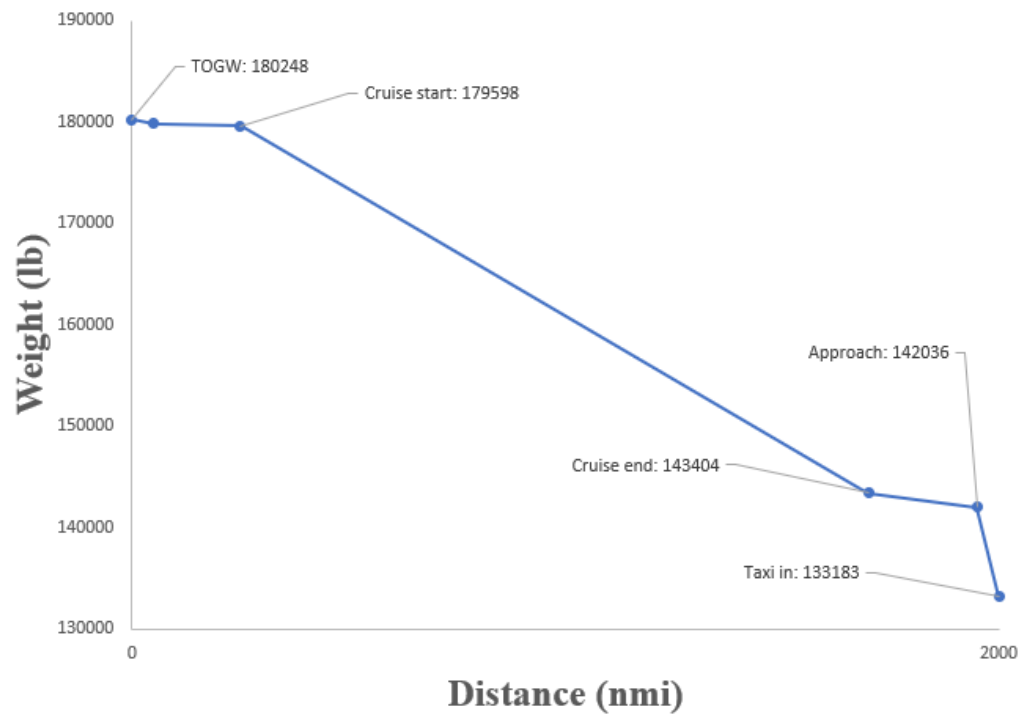


**Fig. 4-2.** Weight propagation profile for full-payload firefighting.

To ensure that our aircraft is designed to meet the 2,000 nmi ferry mission requirement, simulation and estimation was conducted to configure for zero payload and a new design mission range of 2,000 nmi. This new fuel requirement was later compared with maximum fuel capacity to make sure there will be enough propellant to cover the distance. Similar to the firefighting mission, ferry mission profile and weight propagation are shown in Figure 4-3 & 4-4 below.



**Fig. 4-3.** Altitude mission profile for ferry mission.



**Fig. 4-4.** Weight propagation for ferry mission.

## **4.2 Estimation method**

NASA software “Flight Optimization System” (FLOPS) was the main tool used for quantitatively estimating the weight and size of the aircraft. This software requires inputs that can be categorized into three groups: configurational data, operational data, and mission design. As explained in detail below, we obtained these input values from other assisting software, references from existing aircraft, and our understanding of the design requirements or objectives.

### **Configurational data**

After the preliminary solid model of the aircraft was built within the OpenVSP software, geometric information was inputted into FLOPS parametrically to record the basic configurations of the wing, tail, fuselage, fin, gear, and propulsion system. For the wing, major input data included the span, anhedral angle, area, aspect ratio, sweep angle, flap area ratio, number of sections, section span-wise locations, section chord lengths, sectional airfoil thickness-chord ratio, and span-wise engine positions. For the horizontal and vertical stabilizers, important inputs included their corresponding areas, sweep angles, aspect ratios, and taper ratios. Fuselage length, width, and height were also recorded to depict its size. Two fins were added to mimic the winglet design and their area, aspect ratio, taper ratio, sweep angle, and thickness-chord ratio were inputted. A nominal landing gear specification for a similarly sized operating aircraft, such as Boeing 757, was used as a placeholder. Last but not least, the propulsion system was defined by the number of engines, thrust output, and weight.

### **Operational data**

By referencing currently operating firefighting aircraft such as Boeing 737 and DC-10, we determined the appropriate number of flight crews onboard would be three, consisting of one captain, one first officer, and one flight engineer. Some other operational information including performance controls, factors, mission segment definition, ground operations, and takeoff and approach allowances were also determined from operating aircraft of similar class such as Boeing 757 and C-130.

### **Mission design**

Following the mission profile above and the RFP, the climb, cruise, and descent segments were defined by their specific speed, altitude, and rate (Table 4-1). Particularly for cruising conditions, three different schedules were set to cover the high-altitude-high-speed cruise at 20,000 ft and 0.6-0.8 mach, the mid-altitude-mid-speed

preparation flight at 3,000 ft and 0.45 mach, and low-and-slow drop period at 300 ft and 0.23 mach. Mission schedule also defined the multidrop maneuver by specifying two separate 40,000 lb releases.

**Table 4-1** Mission Schedules Defined for FLOPS Input

Segment	Start altitude (ft)	Start speed (Mach)	End altitude (ft)	End speed (Mach)	Notes
START	0	0	0	0.23	Taxi, takeoff
CLIMB	0	0.23	20,000	0.6-0.8	20 nmi
CRUISE 1	20,000	0.6-0.8	20,000	0.6-0.8	350 nmi
CRUISE 2	3,000	0.45	3,000	0.45	20 nmi
RELEASE	300	0.23	300	0.23	1 nmi (drop 1)
CRUISE 3	3,000	0.45	3,000	0.45	10 nmi
RELEASE	300	0.23	300	0.23	1 nmi (drop 2)
CLIMB	300	0.23	20,000	0.6-0.8	20 nmi
CRUISE 1	20,000	0.6-0.8	20,000	0.6-0.8	348 nmi
DESCENT	20,000	0.6-0.8	0	0.23	30 nmi
END	0	0.23	0	0	Landing, taxi

#### 4.3 Estimation results

In the FLOPS output, two vital sections were given high attention for evaluation and analysis: “Output from the weights module” that contains itemized weight breakdown and “Mission summary” that contains important operational information relevant to performance. The estimation for weight and mission parameters was configured that the designed aircraft model is able to achieve the requirements and objectives. Note that the following quantities reported are all approximations to account for the uncertainties in our analytical tools.

##### Operating empty weight (OEW)

As itemized in Figure 4-5, total structural weight was computed to be about 74,500 lbs, including a 36,400-lb wing, a 3,950-lb horizontal tail, a 5,000-lb vertical tail, a 14800-lb fuselage, and a 12200-lb landing gear system. Total propulsion weight was estimated to be around 17,600 lbs, which included two RB211-535 turbofan engines that each added 8200 lbs of dry weight. Total system and equipment weight summed up to about 14,900 lbs

to ensure that there are ample margins for surface control, APU, hydraulics, electrical wiring, avionics, equipment, and instruments. With crews, unusable fuel, engine oil, and cargo containers included, the total operating empty weight was concluded at about 133,000 lbs. This operating empty weight takes up about 55% of the total takeoff gross weight. Double checking the validity of the empty weight estimation with reference aircraft showed that this value is indeed between the Boeing 737 (90,000 lbs) (Modern Airlines, 2022) and DC-10 (240,000 lbs) (Modern Airlines, 2022). Boeing 757 which has a similar size to our aspiration has an operating empty weight about 115,000 lbs, which is also closer to our number (Boeing, 2007). The fact that our empty weight estimation is slightly lower than Boeing 757 can be attributed to different mission profile and possibly a more efficient design.

MASS AND BALANCE SUMMARY	PERCENT WREF	POUNDS
WING	15.02	36424.
HORIZONTAL TAIL	1.63	3948.
VERTICAL TAIL	2.07	5014.
VERTICAL FIN	0.25	606.
CANARD	0.00	0.
FUSELAGE	6.09	14763.
LANDING GEAR	5.02	12169.
NACELLE (AIR INDUCTION)	0.66	1589.
STRUCTURE TOTAL	( 30.72)	( 74512.)
ENGINES	6.76	16404.
THRUST REVERSERS	0.00	0.
MISCELLANEOUS SYSTEMS	0.21	517.
FUEL SYSTEM-TANKS AND PLUMBING	0.28	668.
PROPULSION TOTAL	( 7.25)	( 17589.)
SURFACE CONTROLS	1.06	2560.
AUXILIARY POWER	0.20	490.
INSTRUMENTS	0.23	553.
HYDRAULICS	0.49	1179.
ELECTRICAL	0.69	1667.
AVIONICS	0.65	1570.
FURNISHINGS AND EQUIPMENT	2.32	5631.
AIR CONDITIONING	0.39	957.
ANTI-ICING	0.12	302.
SYSTEMS AND EQUIPMENT TOTAL	( 6.15)	( 14911.)
WEIGHT EMPTY MARGIN	4.12	10000.
WEIGHT EMPTY	48.25	117012.
CREW AND BAGGAGE-FLIGHT, 3	0.28	675.
-CABIN, 0	0.00	0.
UNUSABLE FUEL	0.16	399.
ENGINE OIL	0.07	168.
PASSENGER SERVICE	0.00	0.
CARGO CONTAINERS	6.13	14875.
OPERATING WEIGHT	54.89	133129.

**Fig. 4-5.** FLOPS weight estimation itemized breakdown.



## **Payload weight**

As stipulated in the RFP, this firefighting aircraft should be able to carry at least 4,000 gallons of fire retardant, and a capacity of 8,000 gallons will satisfy the objective. We decided to design the 8,000 gallons for the following reasons. First, the firefighting fleet lacks a relatively new VLAT member that is specifically designed for airtanking mission. All the currently operational air tankers are retrofitted from commercial (eg. DC-10) or military aircraft (eg. C-130), which limits the option and suffers from sub-optimal operational efficiency. The addition of this 8,000-gallon-class VLAT designed to tackle massive wildfire will be demanded in the near future as existing aircraft retire and local governments seek cheaper and more effective wildfire combatting solutions. Second, the large capacity will enable more versatile mission schedules such as multiple drops, direct fire extinguishing, direct fire suppression, indirect fire spreading prevention, and reactions for both scattered and congregated fire sites. Third, the large capacity will increase the effectiveness by a factor of 2 when compared to the Boeing 737 air tanker because in the same mission time frame, our aircraft is able to deliver twice the amount of retardant and still return as fast for refilling for the next mission. Fourth, from the manufacturers' standpoint, the design would be more competitive if it can carry as much payload as possible as long as the operational cost, maintenance cost, and price can be kept reasonable. A lot of affection is given to firefighting helicopters nowadays for their easy field requirement, high efficiency, high mission turn-over rate, and increasing capacity. The Boeing 737 with 4,000 gallons flown from a base airport can usually be swapped with two helicopters from smaller regional airports, which diminishes the cost-effectiveness of using smaller-class air tankers. With reasons stated, we assumed the density of the retardant to be 10 lbs per gallon, which is 11% higher than the floor limit in RFP, hoping to account for more retardant varieties. This concludes to an 80,000-lb cargo weight input in FLOPS and arrives at a zero fuel weight of about 213,000 lbs. This zero fuel weight takes about 88% of the total takeoff gross weight.

## **Mission fuel**

An Engine Deck (ENGDEK) file for FLOPS was made starting with the development of an RB211-535 cycle model in Gasturb about its performance at each flight altitude and speed. With two RB211-535 engines, the total mission fuel was estimated to be 29,400 lbs, which is equivalent to 12% of the total takeoff gross weight.

## Ramp gross weight

Also known as the takeoff gross weight (TOGW) or MTOW, this is the sum of zero fuel weight and total mission fuel weight. For our aircraft, takeoff gross weight was estimated to be about 243,000 lbs (Figure 4-6).

OPERATING WEIGHT	54.89	133129.
PASSENGERS, 0	0.00	0.
PASSENGER BAGGAGE	0.00	0.
CARGO	32.98	80000.
ZERO FUEL WEIGHT	87.88	213129.
MISSION FUEL	12.12	29406.
RAMP (GROSS) WEIGHT	100.00	242535.

**Fig. 4-6.** FLOPS estimation for mission fuel and TOGW.

## Mission summary

As an example for a nominal firefighting mission to the maximum radius (shown in mission profile), we set the schedules as shown in the mission profile in Figure 4-1. Mission summary from FLOPS showcases important information about segment fuel consumption, weight propagation, and time requirement as shown in Figure 4-7 below. The rightmost column indicated the change in altitude of their aircraft in the various stages of the mission.

* * * M I S S I O N S U M M A R Y * * *											
SEGMENT	INITIAL WT(LB)	FUEL(LB)		TIME(MIN)		DIST (N MI)		MACH NUMBER		ALTITUDE(FT)	
		SEGMT	TOTAL	SEGMT	TOTAL	SEGMT	TOTAL	START	END	START	END
TAXI OUT	242535.	434.	434.	10.0	10.0						
TAKE OFF	242101.	217.	650.	0.4	10.4			0.230			0.
CLIMB	241885.	2458.	3108.	5.7	16.1	29.1	29.1	0.230	0.600	0.	20000.
CRUISE	239427.	6874.	9982.	57.0	73.1	350.0	379.1	0.600	0.600	20000.	20000.
CRUISE	232552.	580.	10563.	4.1	77.2	20.0	399.1	0.450	0.450	3000.	3000.
RELEASE	231972.	0.	10563.	0.0	77.2	0.0	399.1	0.450	0.450	3000.	3000.
CRUISE	191972.	374.	10937.	3.9	81.1	10.0	409.1	0.230	0.230	300.	300.
RELEASE	191598.	0.	10937.	0.0	81.1	0.0	409.1	0.230	0.230	300.	300.
CLIMB	151598.	1457.	12394.	3.4	84.5	17.2	426.3	0.230	0.600	300.	20000.
CRUISE	150141.	4971.	17365.	44.5	129.0	273.4	699.7	0.600	0.600	20000.	20000.
DESCENT	145170.	1370.	18735.	29.4	158.5	100.3	800.0	0.600	0.300	20000.	0.
APPROACH	143799.	217.	18952.	1.0	159.5						
RESERVES	143583.	10454.	29406.								
TAXI IN		217.		5.0	164.5						
ZERO FUEL	133129.										

**Fig. 4-7.** FLOPS output mission summary.

According to Table 4-2, the vast majority of the fuel consumption occurs at the initial and final cruise segments at 20,000 ft altitude. This indicates that in-depth designing, testing, and analysis of the major components like wing and fuselage are necessary to ensure optimal aerodynamic, structural, and mission performance. These optimizations will not only make the aircraft more fuel efficient, but will also help minimize the takeoff gross weight and maximize in-flight performances, which will be discussed later in the report.

The mission was estimated to last 2.74 hours with a flight time of 148.1 minutes, covering a design range of 800 nmi, and requiring a block fuel of about 19,200 lbs (Table 4-3).

**Table 4-2.** FLOPS Estimated Segment Fuel Weight Fraction

<b>Segment fuel weight fraction</b>		
<b>Segment</b>	<b>Weight (lb)</b>	<b>Fraction</b>
<b>Taxi out</b>	434	0.0148
<b>Take off</b>	217	0.00738
<b>Climb</b>	2458	0.0836
<b>Cruise 1 (20,000 ft, 0.6-0.8 Mach)</b>	6874	0.234
<b>Cruise 2 (3,000 ft, 0.45 Mach)</b>	580	0.0197
<b>Release 1</b>	0	0
<b>Cruise 3 (300 ft, 0.23 Mach)</b>	374	0.0127
<b>Release 2</b>	0	0.00
<b>Climb</b>	1457	0.0496
<b>Cruise 1 (20,000 ft, 0.6-0.8 Mach)</b>	4971	0.169
<b>Descent</b>	1370	0.0466
<b>Approach</b>	217	0.00738
<b>Reservers</b>	10454	0.356
<b>Taxi in</b>	217	0.00738
<b>Total</b>	29406	1

**Table 4-3.** Auxiliary Mission Summary Information

<b>Mission summary</b>	
Design range (nmi)	800
Flight time (min)	148.1
Block time (hr)	2.74
Block fuel (lb)	19170
ATA traffic allowance (nmi)	70.3

## 5. Matching Plots

In the preliminary sizing process, we generated a matching plot based on estimated thrust-weight ratio (T/W) and wing loads (W/S). Our goal was to determine the optimal point within the working range that achieved the lowest T/W and the highest W/S. In order to do this, six constraints related to the stall speed, takeoff field length, landing field length, cruise speed, rate of climb, and sustained loading factor were accessed. The equations (one through six) that were used in this process came from the *Fundamentals of Aircraft and Airship Design: Volume 1* textbook written by Nicolai, L. M., & Carichner (2010), which are listed below in the requirements and constraints section .

### 5.1 Requirements and Constraints

1. Stall Speed Constraint

$$\frac{W}{S} \leq \frac{1}{2} \rho V_{stall}^2 C_{Lmax} \quad \text{Eqs. (1)}$$

2. Takeoff Distance Constraint

$$\frac{T}{W} = \frac{20.9 \left( \frac{W}{S} \right)}{\sigma C_{Lmax} \left( S_{TO} - 69.6 \sqrt{\frac{\left( \frac{W}{S} \right)}{\sigma C_{Lmax}}} \right)} \quad \text{Eqs. (2)}$$

3. Landing Distance Constraint

$$\frac{W}{S} = \frac{\sigma C_{Lmax}}{79.4} \left( S_L - \frac{50}{\tan \theta_{APP}} \right) \quad \text{Eqs. (3)}$$

4. Cruise Speed Constraint

$$\frac{T}{W} = \frac{q C_{D0}}{\left( \frac{W}{S} \right)} + \frac{\left( \frac{W}{S} \right)}{q \pi A Re} \quad \text{Eqs. (4)}$$

5. Rate of Climb Constraint

$$\frac{T}{W} = \frac{P_s}{V} + \frac{1}{\frac{L}{D}} \quad \text{Eqs. (5)}$$

6. Sustained Load Factor Constraint

$$\frac{T}{W} = \frac{nD}{L} = \frac{n}{\frac{L}{D}} \quad \text{Eqs. (6)}$$

## 5.2 Justification for input values

Justification for input values can be supported by focusing on the climbing, cruising, and loitering stages. After conducting basic research on basic conditions, we know that this aircraft will generally be cruising at about 450 knots (231.5 m/s), at an altitude of 10,000 ft, and the air density at this altitude will be around  $0.91 \text{ kg/m}^3$ . When looking at the climb phase, L/D ratios should be considered as it will focus on reducing the time to climb while maximizing the flight path angle. For L/D, we used a nominal value of 26 because this is usual for heavy transport aircraft. Using data sourced from Aircraft Design by J. A. Schetz,  $C_{D0}$ ,  $C_{Lmax}$  and other airfoil-specific values such as  $e$  and AR related to NACA 6412 were determined and listed below in Table 5-1. Assumptions for the velocity values,  $S_{TO}$  and  $S_L$ , and  $\theta_{APP}$  were determined from research and interpolation from specification for the DC-10 aircraft. In regards to the stall speed,  $V_{stall}$ , when researching we agree that this value has to be lower than 150 knots in order to meet the payload drop speed requirement, and lower than lower than 125 knots to meet the objective, therefore we chose 110 knots or 185.659 ft/s as our value. The airfoil we chose was the NACA 6412, and this particular airfoil can produce a  $C_{L,max}$  coefficient of around 1.48. In regards to the air density ratio,  $\sigma$ , this value was calculated to be equal to 0.8617 due to the RFP field requirement of 5,000 ft MSL. For the aspect ratio (AR), we were able to calculate this value in OpenVSP due to it being equal to  $span^2/planform\ area$ , which we found to be equal to 15.54. This also allowed us to calculate the wing efficiency factor, ( $e$ ), for a semi-symmetrical wing with  $AR = 15.54$  to be about 0.85. For the specific excess power, the calculated number is comparable with the nominal value of 100 ft/s.  $V_{TOC}$ , it is calculated with cruising Mach of 0.75 at the top-of-climb altitude of 35,000 ft.

**Table 5-1.** Constraint Calculation Chart

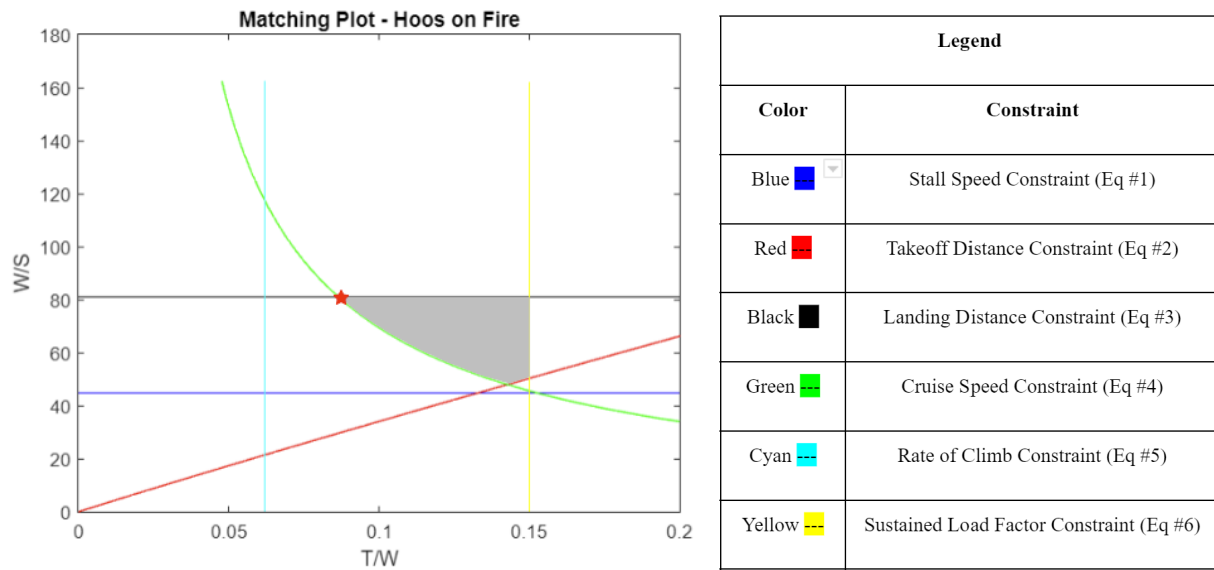
$\rho$ (slugs/ft <sup>3</sup> )	$17.56 \times 10^{-4}$ (10,000 ft)	$e$	0.85
$C_{D0}$ (airfoil data)	0.007	$S_{TO}$ (ft)	6,000
$K$	0.036	$\theta_{APP}$	4.5
$C_L$	0.8	$S_L$ (ft)	6,000
$V$ (ft/s)	860.78	$P_S$ (ft/min)	100
$C_{Lmax}$ (airfoil data)	2.21 @-30 deg	$V_{Top-of-climb}$ (ft/s)	794.36
$V_{STALL}$ (ft/s)	185.66	$L/D$	26
$\sigma$	0.8617	$T_{max}$ (lbf)	44,800
$q$ (lbf/ft <sup>2</sup> )	966.9	$n$	2.5
$AR$	15.54		

### 5.3 Results Explanation

Seen in Figure 5-1, the region chosen for sizing was based on convergence of functions and constraints from the inequalities above. The yellow highlighted region designates the area for design. In this region, the aircraft satisfies all constraints given by the plotted equations. The various constraints are depicted in different colors which are identified in the legend. This design region on each plot met the following requirements: a wing loading ( $W/S$ ) above the stall speed constraint, a thrust loading ( $T/W$ ) less than the takeoff distance constraint, a  $W/S$  less than the landing distance constraint, a  $T/W$  greater than the cruise speed constraint, a  $T/W$  greater than the rate of climb constraint, and a  $T/W$  below the sustained load factor constraint. This region can be used to design an aircraft that optimizes different parameters. For example, to optimize maneuverability, the aircraft should be designed to have a lower  $W/S$  in the selected range.

Within this region, a single point was selected that maximized  $W/S$  while minimizing  $T/W$  which maintains that the value is large enough to optimize air range per unit fuel; this point is shown by the green arrow. It also

guarantees  $W/S$  is not too large so that maneuverability and takeoff and landing distance are not sacrificed, which ensures that the desired characteristics of the aircraft can be achieved at a chosen size and thrust configuration.



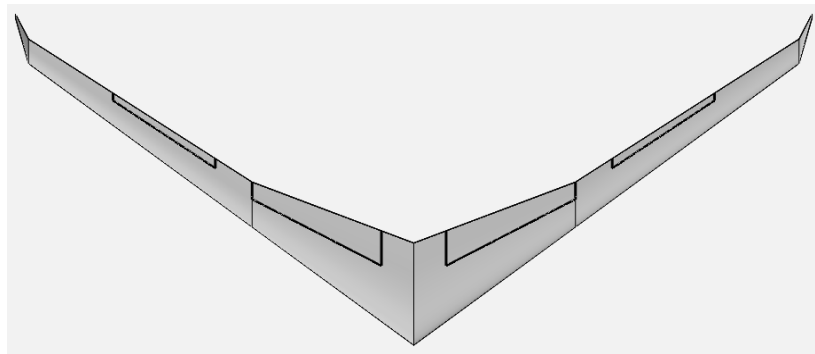
**Fig. 5-1.** Design space for Material Girl (grey). Red star is the minimum  $T/W$  and maximum  $W/S$ .



## 6. Wings

### 6.1 Design Overview

We arrived at the final wing design with a ultra-high-AR, high-mounted anhedral wing with high-lift control surfaces and canted winglets (Figure 6-1). The wing has a slender planform area to reduce the effect of finite-wing induced drag. It carries one flap and one aileron on each side symmetrically to assist with roll maneuver and lift generation at low speeds respectively. The wing on each side is segmented into two sections to achieve ultra-high AR and maintain structural rigidity at the wing-fuselage integration. Detailed metrics are summarized in Table 6-1.



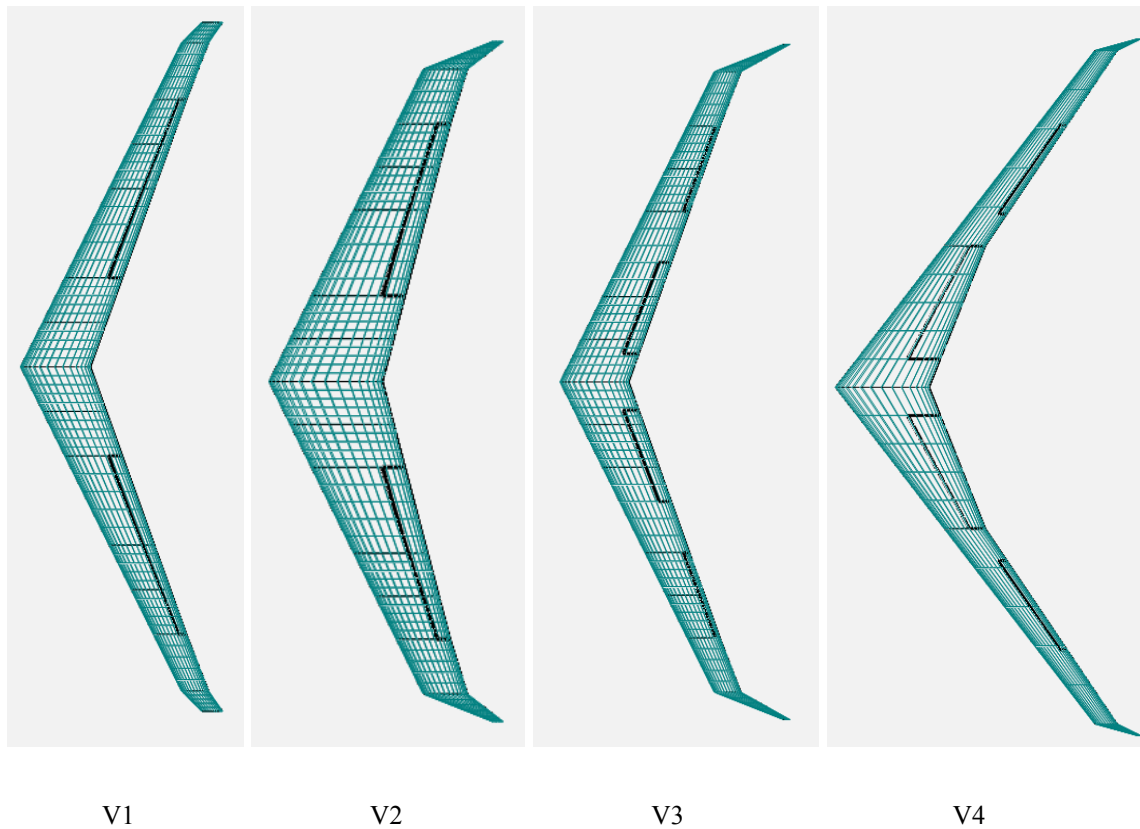
**Fig. 6-1.** Overhead view of wing

**Table 6-1.** Wing Parameters

	Section 1	Section 2	Winglet	Total
Area ( $ft^2$ )	1432.80	935.71	45.06	2413.57
Airfoil	NACA 6412	NACA 6412	NACA 6412	—
Projected Span (ft)	79.56	110.02	6.44	196.02
Sweep	36°	36°	60°	—
Dihedral	-2°	-2°	60°	—
Aspect Ratio	4.42	12.94	1.83	15.54
Root Chord (ft)	25	11	6	—
Taper Ratio	0.440	0.545	0.167	—
MAC (ft)	18.91	8.75	4.10	14.79

## 6.2 Design Approach

There were four design iterations for the wing, seen below in Figure 6-2. The initial wing design had a uniform geometry and featured winglets at the end. The final design improved on this, resulting in two distinct segments and keeping the winglets. The iterations improve from left to right and rightmost picture as our final choice.



**Fig. 6-2.** Design evolution of wing

Trade studies were utilized in the wing optimization process. Table 6-2 below outlines the various parameter variables, corresponding to wing design iteration, that were compared using simulation outputs. When designing the wing, we knew that it must generate substantial amounts of lift to keep an air tanker class aircraft in the air. Thus, a large surface area was prioritized, as well as a sweep angle to allow for faster flight in the early design phases. We also wanted to optimize performance by increasing the aspect ratio as much as allowable, and including winglets to reduce induced drag. OpenVSP and FLOPS were used to inform our choices for the wing parameters shown in Table 6-1 above. Initially, we used a sweep angle of  $25^\circ$ , a span of 175.02 feet, and an area of

2020.52 square feet in Version 1 (V1). The basis for these values was produced by a FLOPS sizing and mission analysis on weight, fuel burn, and mission performance for each configuration. VSPAERO was then used to analyze the aerodynamic performance given these parameters. V1's area and chord length, however, were less than optimal and these parameters were increased for V2, as well as increasing the winglet sweep and taper. V2 gave us plenty of lift through its increased area (2320 ft<sup>2</sup>) and chord length (30 ft), but this was at the cost of additional weight (53,000 lbs). Both V1 and V2 utilized large flaperons for increased maneuverability and maximum coefficient of lift, with V2 increasing the percentage of chord length from 15% to 25%. While V1 and V2 gave us good bounds for consideration, V3 struck a balance between the two by giving us our desired aspect ratio, as well as splitting the flaperons into flaps and flaperons to increase the maximum coefficient of lift (CL<sub>max</sub>). VSPAERO was used to determine the aerodynamic characteristics, and the CL<sub>max</sub> was not sufficient for the stall speed being below the desired drop speed of 125 knots. There were also worries over whether the wing would be structurally sound with such a large aspect ratio. The V4 wing optimized the sweep angle, aspect ratio, and area for the best aerodynamic performance from VSPAERO and the least fuel burn as our FLOPS estimation was further refined. We found it necessary for V4 to add an interior section with increased chord length to support the wing weight. This allowed us to keep the large aspect ratio and its added performance benefits while still being safe to fly. The flap and flaperon percentage was increased from V4 due to the increased sweep that FLOPS informed us would decrease the block fuel burn. This increase was necessary to produce the CL<sub>max</sub> needed to meet our objective of a drop speed below 125 knots.

**Table 6-2. Wing Version Comparison**

Variable Parameter	Design			
	V1	V2	V3	V4
Aspect Ratio	15.16	9.41	15.52	15.54
Projected Span (ft)	175.02	138.35	175.24	196.02
Area (ft <sup>2</sup> )	2020.52	2033.64	1978.55	2413.57
Sweep	25°	25°	25°	36°
Flaps	—	—	25%	40%
Flaperons	15%	25%	15%	25%

### 6.3 Wing position

Table 6-3 below depicts the location of the wing. The wing's horizontal position was chosen to center the CG near the middle of the fuselage and to provide a suitable static margin throughout the mission. We used OpenVSP to adjust its location and determine the aerodynamic center through several iterations until it was positioned aft of the CG. This configuration ended up being ideal over the range considered (30 – 60 ft from nose) with a static margin of 6.09% (further discussed in section 11.8). This position of the wing was chosen to match with the vertical and horizontal stabilizers based on the available space on the fuselage. These coordinates in relation to each other ensured our aircraft was statically stable. To provide maximum visibility for the pilot, the engines were kept out of the line of sight and the wings were positioned as far back as possible while still being stable (in addition to their sweep). Further discussion of CG travel, static margin, and stability considerations will be discussed later.

**Table 6-3.** Wing position

<b>X location (measured from nose) [ft]</b>	45.9
<b>Z location (measured from fuselage centerline) [ft]</b>	3.54

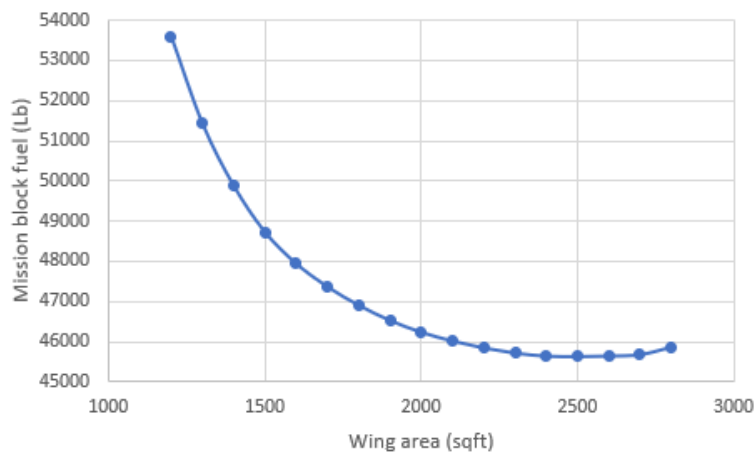
The wing's vertical location was chosen to be high-mounted with an anhedral angle to provide the pilot with the most visibility while still being a stable configuration for aerodynamics. The anhedral angle of  $2^\circ$  was chosen to improve visibility, ground clearance, and maneuverability. We arrived at this value through FLOPS weight and mission data coupled with OpenVSP aerodynamic performance and stability data. The high-mounted anhedral wing is inherently more unstable than low-mounted dihedral configurations, and this lets our aircraft produce higher roll rates for maneuvering during missions. A previous iteration used an anhedral angle of  $4.84^\circ$ , but this did not satisfy our ground-clearance constraint under a 2g hard landing and was less stable during cruise than a  $2^\circ$  anhedral angle. This anhedral angle struck a balance between a necessary stability and our desired maneuverability.

### 6.4 Fundamental wing geometric configurations

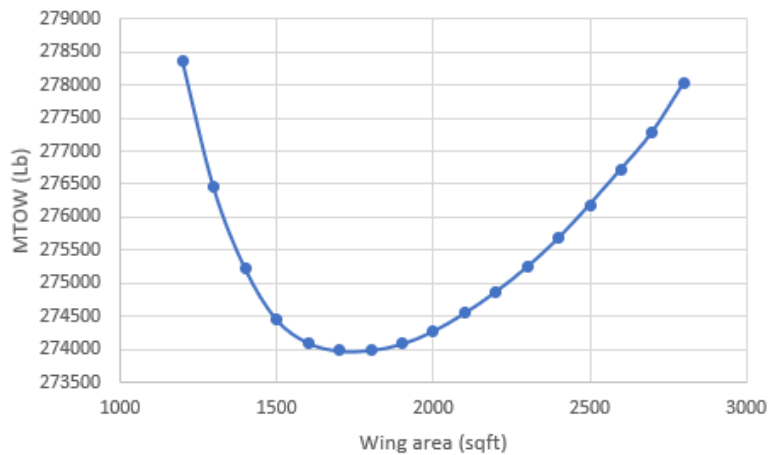
The wing is one of the largest structural components in the aircraft and its design has a huge impact on both aerodynamic performances and sizing, manifested as fuel consumption and takeoff gross weight respectively. With two major design criteria in mind, minimizing takeoff gross weight and minimizing fuel consumption, three trade studies were identified: wing area, wing sweep angle, and wing aspect ratio (AR).

## Wing area trade studies

According to the two reference air tankers currently in operation, Boeing 737 is able to carry 4,000 gallons of retardant and that for DC-10 is 12,000 gallons. Our design objective at 8,000 gallons is right in the midpoint of the spectrum. Aircraft size is assumed to have a linear relationship with their cargo capacity, which makes our aspired wing area within the range between 1350 and 3550 square feet. FLOPS was used to iterate through these values after which total mission fuel and takeoff gross weight were plotted as a function of the wing area, as shown in Figure 6-3 & 6-4 below:

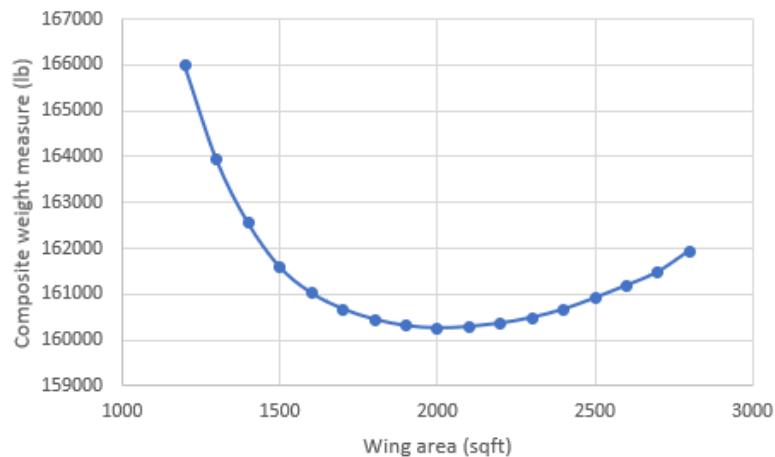


**Fig. 6-3.** Block fuel burn vs Wing area



**Fig. 6-4.** Maximum takeoff weight vs Wing area

Note that fuel consumption and takeoff gross weight are minimized at slightly different values for wing area. To finalize the optimal wing area, these two criteria were equally weighted by 50% to evaluate for the overall relationship, as shown in Figure 6-5, where the local minimum falls around 2,000 square feet.






**Fig. 6-5.** Block fuel burn & Maximum takeoff weight vs Wing area with equal weighting

This optimized wing area seems reasonable because it falls between the areas of Boeing 737 and DC-10. Further comparison with the Boeing 757, which has almost the same cargo capacity and a wing area of 1994 square feet, confirms the analysis.

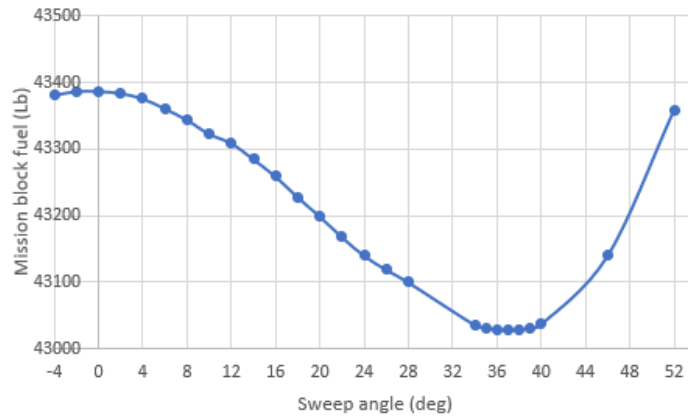
### Wing sweep angle trade studies

Wing sweep angles generally fall in three domains: negative (forward sweep), zero (no sweep), and positive (backward sweep). Three reference aircraft were considered: X-29, C-130, and Boeing 777. Table 6-4 organizes these aircraft and their characteristics.

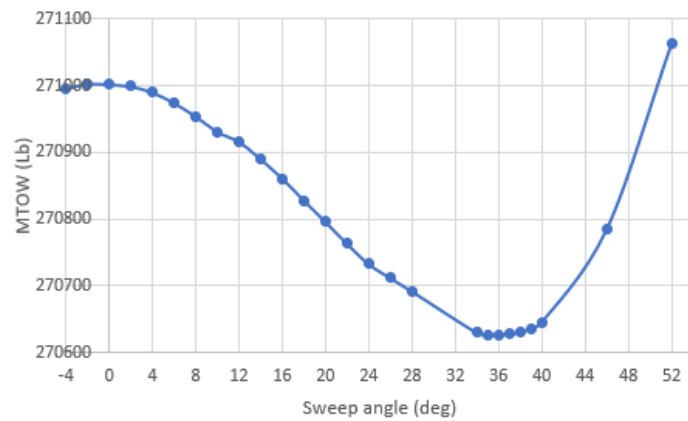
**Table 6-4.** Comparator Aircraft for Wing Sweep

Reference aircraft	Wing sweep angle	Comment
	-33 deg	<ul style="list-style-type: none"><li>• Experimental</li><li>• Better stall maneuverability</li><li>• Unstable to control</li></ul>
	0 deg	<ul style="list-style-type: none"><li>• Operating</li><li>• Relatively older design</li><li>• Slower cruising speed</li><li>• Structurally efficient</li><li>• Flow separation</li></ul>
	+31.64 deg	<ul style="list-style-type: none"><li>• Operating</li><li>• Relatively newer design</li><li>• Transonic flight capable</li><li>• Help with efficiency</li><li>• Stricter margin for size and material</li></ul>

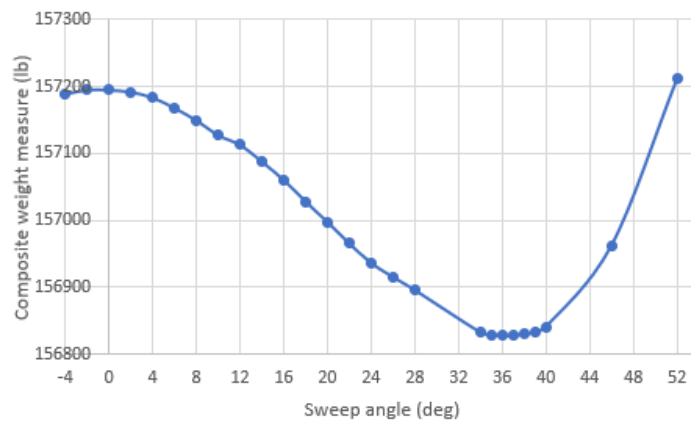
We decided to set the test range to  $-4 \sim +52$  degrees to cover for as many designs as possible and necessary. FLOPS was used again to perform a similar analysis on wing sweep angle influence on the mission fuel and takeoff gross weight, as shown in Figure 6-6, 6-7, & 6-8 below. We then concluded that the local minimum (optimized sweep angle) was at 36 degrees. This value makes sense as it is close to most of the latest commercial aircraft designs such as Boeing 777 (31.64 deg), Boeing 787 (32.2 deg), and Airbus 350 (31.9 deg). It is slightly higher than these operating models, but this can be attributed to two explanations: a) FLOPS is an estimation tool that simulates under ideal conditions, so it is not capturing the exact fluid dynamics or aeroelastic performances, and b) the trend of having higher sweep angle somewhat agrees with the developmental history as new technology and material became available for aviation, as seen in Airbus 320 (25 deg)  $\rightarrow$  Airbus 350 (31.9 deg) or Boeing 737 (25 deg)  $\rightarrow$  Boeing 787 (32.2 deg). However, we do need to acknowledge the possibility of this sweep angle being unrealistically high for the designed flight speed due to the analytical nature of FLOPS. FLOPS yields estimations based on theoretical equations and empirical data, which may not accurately reflect the weight constraints from aeroelastic, material, or maintenance aspects. Future multi-perspective analyses using high fidelity simulations and experiments are highly recommended to corroborate a sound sweep angle design.



**Fig. 6-6.** Block fuel burn vs Sweep angle



**Fig. 6-7.** Maximum takeoff weight vs Sweep angle

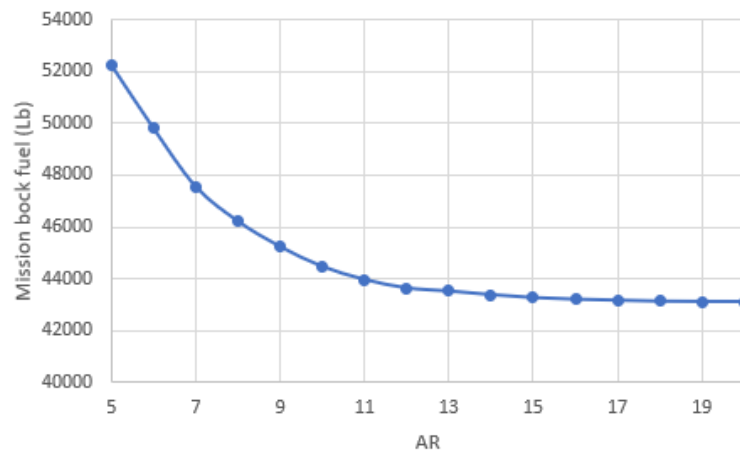


**Fig. 6-8.** Block fuel burn & Maximum takeoff weight vs Sweep angle with equal weighting

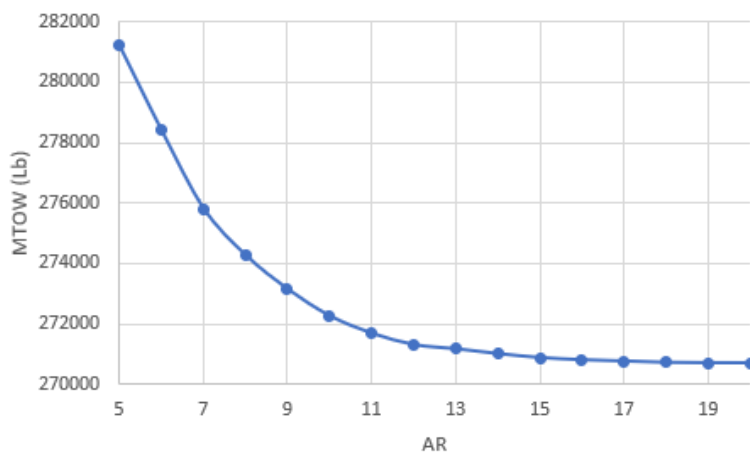


## Wing aspect ratio trade studies

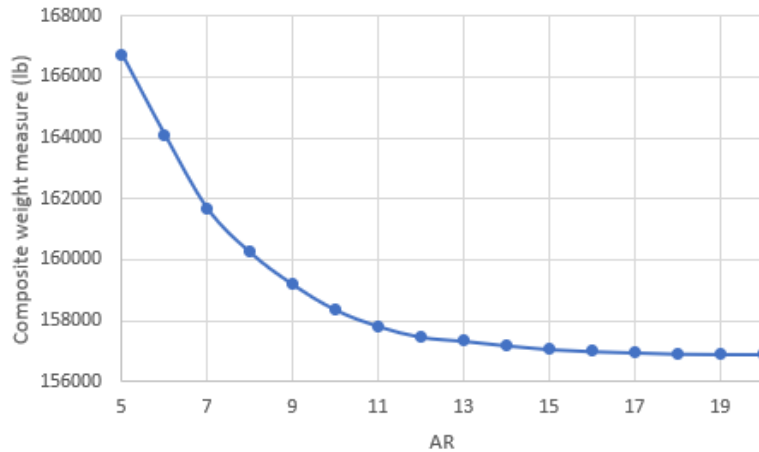
Increasing the wing aspect ratio has been thought to be a way to increase efficiency because it shrinks down the induced drag term due to finite wing. Some efforts have been documented in the aviation industry and academia, such as the concept of Boeing SUGAR VOLT which essentially stretches a Boeing 737 wing from  $AR = 9$  to  $AR = 18$ . We did similar FLOPS analysis by iterating through  $AR = 5$  to 20 and evaluating the effects on fuel consumption and takeoff gross weight. Results are shown in Figure 6-9, 6-10, & 6-11.



**Fig. 6-9.** Block fuel burn vs Aspect Ratio



**Fig. 6-10.** Maximum takeoff weight vs Aspect Ratio







**Fig. 6-11.** Block fuel burn & Maximum takeoff weight vs Aspect Ratio with equal weighting

Initially, we were convinced that the wing aspect ratio optimizes after reaching about 13 according to the plots, hence the design of a long and slender wing planform. However, FLOPS sizing regressions are informed largely by existing, low-AR winged aircraft. Hence, the trust region for the FLOPS weight estimation regressions does not extend much higher than about AR 10-11, and any results above this AR likely do not account for significant sizing impacts due to dynamic aeroelastic sizing loads, which would serve to increase the wing weight - and decrease overall aircraft performance - relative to the FLOPS results shown here. Ultra high aspect ratio can theoretically benefit the aerodynamic performance, but it could be limited by aeroelastic and material concerns. Therefore, further Finite Element Analysis (FEA) was conducted to test for stresses and deformations under extreme loading conditions. FEA analysis and results will be presented in later sections.

## 6.5 Airfoil selection

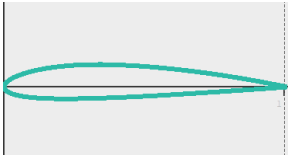

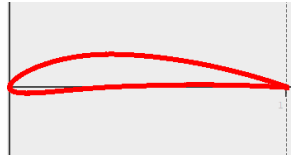

Five airfoil types were initially considered for the wing design, including under-cambered, flat-bottom, semi-symmetrical, symmetrical, and reflexed. Their common applications in reality and their theoretical pros and cons were evaluated, and the top two promising types were determined to be under-cambered and semi-symmetrical, as shown in Table 6-5 below.

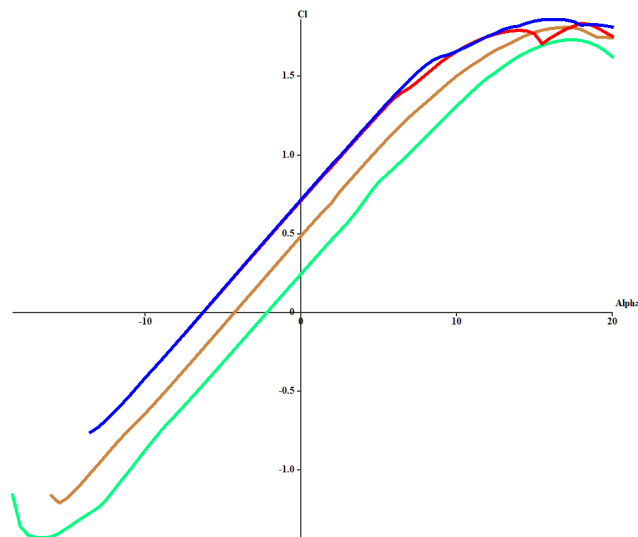
**Table 6-5.** Comparison of Airfoil Types

Type	Image	Pros	Cons
Under-cambered		Good for slow flight; High lift generation	High drag from wake
Flat-bottom		Easily manufactured Decent lift	Relative high drag
Semi-symmetrical		Best lift to drag ratio	More common for sport and aerobatic planes
Symmetrical		Same lift generated in up and down directions	Mainly used for precise aerobatic planes
Reflexed		Auto stability correcting property	Mainly used for flying wings and gliders

To balance the benefits of using either airfoil types, we sought an airfoil on the transitional spectrum from under-cambered to semi-symmetrical shapes, and conducted basic aerial performance simulation in Xflr5 to compare their lift and drag coefficients. In this design cycle, four airfoils were chosen: NACA 2412, NACA 4412, NACA 6412, NACA 6409, ranked from the least under-cambered to the most under-cambered. These airfoils are shown in Table 6-6. Simulations were performed with  $Re = 3E+6$  and swept across  $-20$  to  $+20$  degrees for the angle of attack with an increment of  $0.5$  degree, assuming a 2D geometry without finite wing influences. Results are shown in Figure 6-12, 6-13, & 6-14.

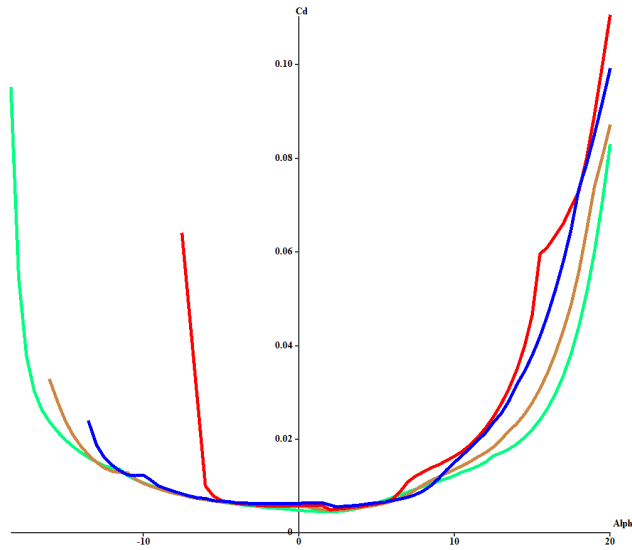
**Table 6-6.** Comparison of Airfoil Geometries

NACA 2412	NACA 4412	NACA 6412	NACA 6409
			



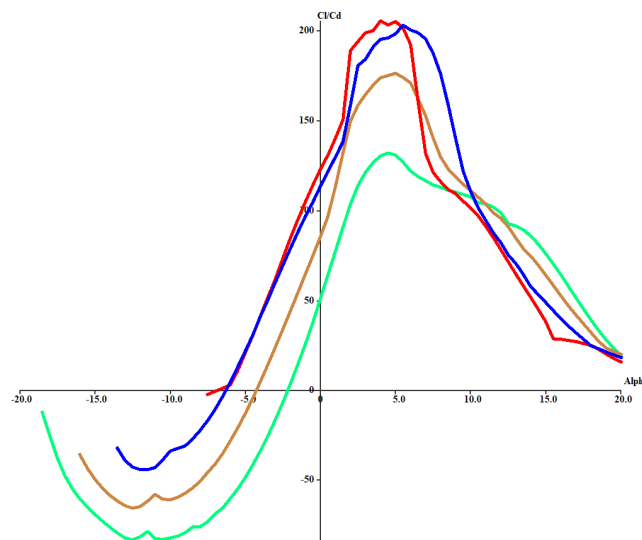
**Fig. 6-12.**  $C_l$  vs.  $\alpha$

NACA 6412 (red curve) shows the highest lift coefficient maximizing around 16 degrees of angle of attack. It also outputs a more reliable lift coefficient than NACA 6409 at high angles of attack.



**Fig. 6-13.** Cd vs. alpha

All four airfoils seem to provide similar drag performance. Note that NACA 6409 airfoil has an earlier Cd increase as the angle of attack enters the negative domain, which corresponds to its tendency for flow separation as the angle of attack increases in the negative direction.



**Fig. 6-14.** Cl/Cd vs. alpha

NACA 6409 and NACA 6412 output the highest lift to drag ratio. This ratio optimizes at around 6 degrees for NACA 6412.

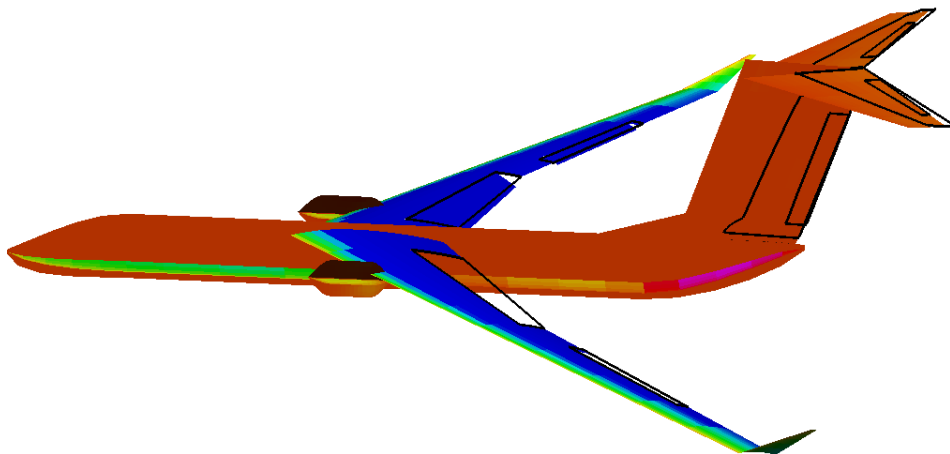
With the airfoil analysis, we determined that NACA 6412 provides the best overall aerodynamic performance by generating high lift with the relatively large camber and avoiding excessive drag build-up with the moderate under-camber amount. This same airfoil was used across the entire wing for two considerations: smooth and uniform surface shape in contact with the wind, and easier manufacturing.

The NACA 6412 airfoil has the max thickness 12% at 30.1% chord and the max camber 6% at 39.6% chord. While providing the best performance out of the airfoils considered, it also has ample space for fuel storage and subsystems within the wing. Its shape is beneficial to structural strength as well since there is more space for material to resist bending, torsion and buckling.

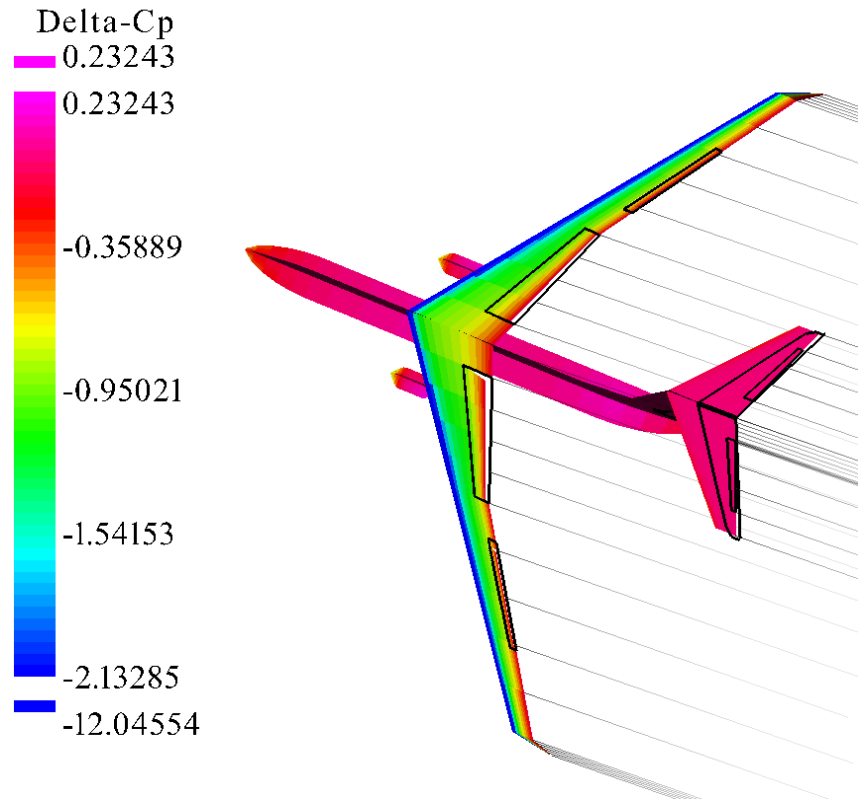
## **6.6 Aerodynamic surfaces**

### **Flaps and Flaperons**

Regular flaps were included in the inner section of the wing, taking up 40% of the local chord length and spanning 95% of the section. These flaps deflect at  $-10^\circ$  and  $-20^\circ$  during approach and landing, and  $-30^\circ$  for low & slow flight during payload deployment. Flaperons were utilized as well in the outer section of the wing, accounting for 25% of the chord and spanning 45% of the section. These flaperons operate on standard hinges, and are capable of being deflected up and down from  $30^\circ$  to  $-30^\circ$  for maneuvering and extra lift during the payload drop and landing. The landing and slow flight configuration can be seen in Figure 6-15 and 6-16, respectively.



**Fig. 6-15.** Deployment of Flaps and Flaperons



**Fig. 6-16.** Landing configuration

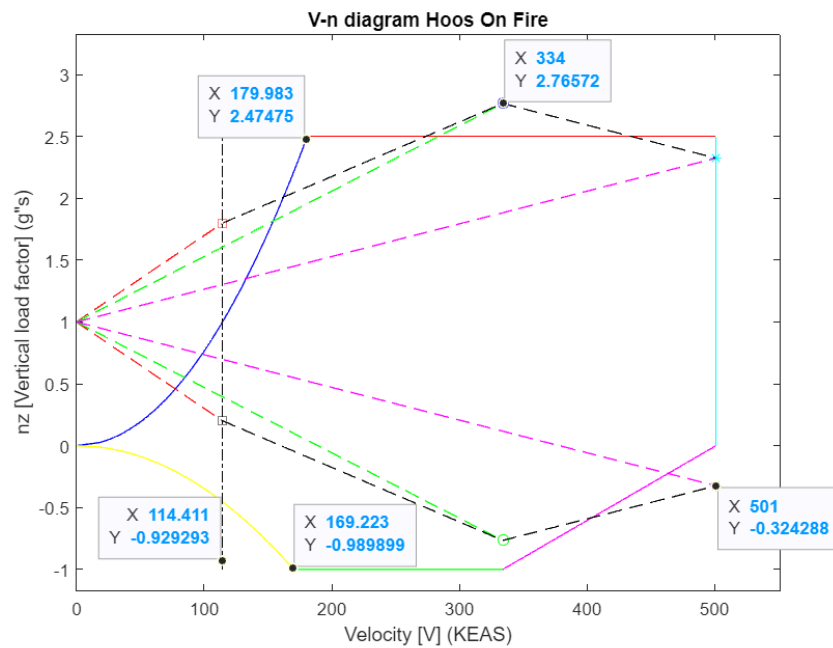
### Winglets

The wings have blended winglets on the end, which reduce the strength of the wingtip vortices, decreasing drag and increasing fuel efficiency. The benefits of these for a large air tanker design outweigh the added weight and skin friction drag. Air tankers require large amounts of lift, which increases the strength of the vortices, so the decrease in induced drag caused by adding winglets will make it more efficient and save fuel over its lifetime. The sweep angle and dihedral angle are designed to provide the seamless transition from the main wing section that a blended winglet would.

### 6.7 Maneuvers

The V-n diagram for the Material Girl is shown below in Figure 6-17. The solid lines represent the flight envelope our aircraft must stay within to prevent permanent structural damage or catastrophic failure. In it, we found the stall speed, corner speed, and dive speed based on our cruise capabilities and maximum coefficient of lift. The

stall speed is in 1 g level flight 114.4 knots, below the 125 knots drop speed objective. The maximum corner speed our aircraft can undergo is 180 knots with a positive sustained load of 2.5 g's. Under a sustained loading of -1 g, we must maneuver at a lower speed of 169.2 knots. When gusts are taken into account, represented by the dashed lines, we found that the maximum positive sustained load we must factor into our analysis was 2.77 g's at the cruise speed of 334 knots. It must also be noted at the dive speed of 501 knots, we must not exceed 2.5 g's or -0.325 g's. This V-n diagram informed our FEA analysis and material selection.



**Fig. 6-17.** V-n diagram for Material Girl

## 6.8 FEA modeling

To resolve the concern about our long and slender wing design from the ultra high aspect ratio, SolidWorks Finite Element Analysis (FEA) was performed to verify structural rigidity and ground clearance under deformation. In each static simulation, half of the wing was constrained as a cantilevered beam at the center cross section. External loads considered include structural gravity (-z), distributive lift (+z), distributive fuel weight (-z), and engine weight (-z). Four scenarios were tested to ensure that the wing is operable under extreme cases. Note that we assumed the wing to be a hollow aluminum shell, and thus we adapted the material density based on the FLOPS-estimated structural weight and the SolidWorks-calculated volume so that gravity is correctly calculated.

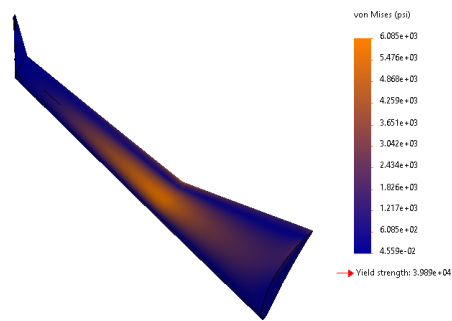


## 1. Takeoff with full payload (Fig. 6-18 & 6-19)

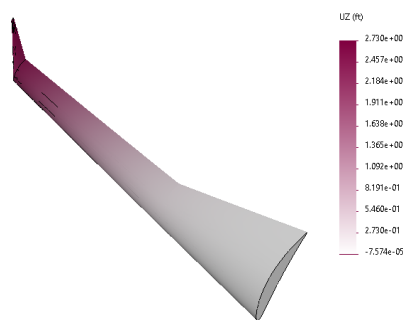
This is simulating a regular takeoff with full payload. Below, Fig. 6-18 depicts the distribution of Von Mises stress on the wing. Additionally, Fig. 6-19 depicts the range of deformation on the wing.

### External loads:

- Structural gravity: 18200 lbs ( $g = 9.81 \text{ m/s}^2$  | density =  $0.00726 \text{ lb/in}^3$  hollowed wing)
- Lift:  $\text{TOGW}/2 = 121,300 \text{ lbs}$
- Fuel weight = Mission fuel/2 = 14,700 lbs
- Engine weight = 8,200 lbs



**Fig. 6-18.** Von Mises stress for full-payload takeoff



**Fig. 6-19.** Wing flex deformation for full-payload takeoff

### Results:

- Von mises stress:  $6.09\text{E}+3 \text{ psi} < \text{yield strength of } 3.99\text{E}+4 \text{ psi}$

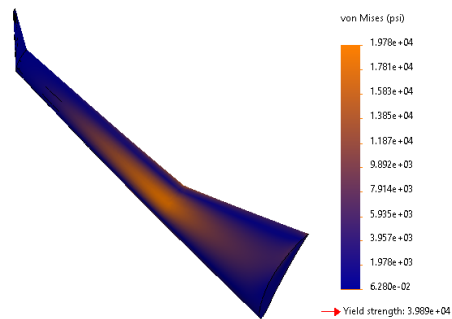
- Wingtip flex displacement: 2.75 ft in +z direction

## 2. Maximum critical load during flight: 2.77 g's (Fig. 6-20 & 6-21)

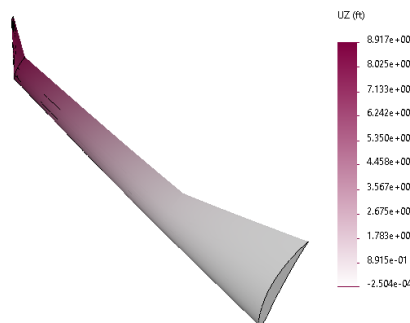
This is simulating an unexpected gust during cruise causing 2.8 times the regular maximum lift. Fig. 6-20 depicts the distribution of Von Mises stress on the wing for a maximum critical load. Additionally, Fig. 6-21 depicts the range of deformation on the wing for the maximum critical load.

### External loads:

- Structural gravity: 18200 lbs ( $g = 9.81 \text{ m/s}^2$  | density =  $0.00726 \text{ lb/in}^3$  hollowed wing)
- Lift:  $\text{TOGW}/2 * 2.8 = 339500 \text{ lbs}$  (critical load from Vn diagram)
- Fuel weight = 14700 lbs
- Engine weight = 8200 lbs



**Fig. 6-20.** Von Mises stress for 2.77g's maximum critical load.



**Fig. 6-21.** Wing flex deformation for 2.77g's maximum critical load.

### Results:

- Von mises stress:  $1.98\text{E}+4$  psi < yield strength of  $3.99\text{E}+4$  psi
- Wingtip flex displacement: 8.92 ft in +z direction

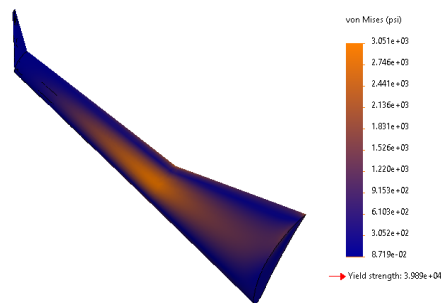
### 3. 2 g ramp bump (Figure 6-22 & 6-23)

This is simulating a bump on the ground during taxi in or taxi out, adding twice the gravity on the structure.

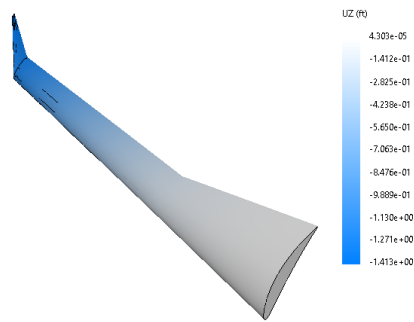
Below, Fig. 6-22 depicts the distribution of Von Mises stress on the wing for ramp bump. Fig. 6-23 shows the range of deformation on the wing for ramp bump.

### External loads:

- Structural gravity: 36400 lbs ( $g = 19.60 \text{ m/s}^2$  | density =  $0.00726 \text{ lb/in}^3$  hollowed wing)
- Lift: 0 lbs (not in flight)
- Fuel weight = 29400 lbs (2g forcing)
- Engine weight =  $8200 \times 2 = 16400$  lbs (2g forcing)



**Fig. 6-22.** Von Mises stress for 2g ramp bump.



**Fig. 6-23.** Wing flex deformation for 2g ramp bump.

**Results:**

- Von mises stress:  $3.05\text{E}+3$  psi < yield strength of  $3.99\text{E}+4$  psi
- Wingtip flex displacement: 1.41 ft in -z direction

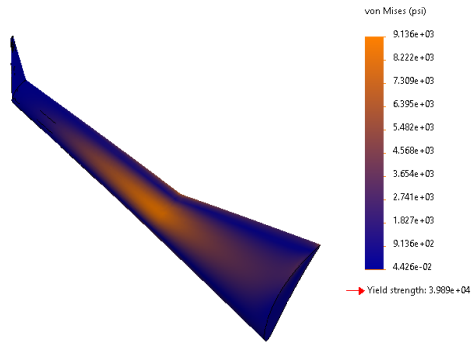
**4. -1 g pull-up loading (Figure 6-24 & 6-25)**

This is simulating the wing loaded with lift forces in the negative z direction during a pull-up maneuver.

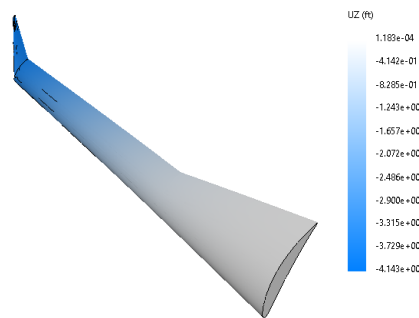
Below, Fig. 6-24 depicts the distribution of Von Mises stress on the wing during pull-up loading. Fig. 6-25 depicts the range of deformation on the wing during pull-up loading.

**External loads:**

- Structural gravity: 18200 lbs ( $g = 9.81 \text{ m/s}^2$  | density =  $0.00726 \text{ lb/in}^3$  hollowed wing)
- Lift: -121300 lbs (negative lift)
- Fuel weight = 14700 lbs
- Engine weight = 8200 lbs



**Fig. 6-24.** Von Mises stress for -1g pull up.



**Fig. 6-25.** Wing flex deformation for -1g pull up.

## Results

- Von mises stress:  $9.14\text{E}+3$  psi < yield strength of  $3.99\text{E}+4$  psi
- Wingtip flex displacement: 4.14 ft in -z direction

All of the FEA results indicate that the ultra high aspect ratio wing is indeed operable in that:

- No stress concentration exceeds the yield strength of 6061 T6 aluminum
- Wingtip deformations in the +z directions are well below the extreme case (documented by Boeing with their Boeing 787 test up to 25 ft)
- Wingtip deformation in the -z direction guarantees ample ground clearance

## 6.9 Summary

Note that these analyses were done under the assumption that the entire wing is made of 6061 T6 aluminum, so values are calculated or compared with its particular material properties. Modern aircraft tend to use more composite materials such as polycarbonate, which usually yields even better mechanical properties than the aluminum, so we concluded that this wing design is supported by the FEA results. Future analysis would include a structural model of the internal supporting structures such as ribs, spars, and webs. We believe these could be designed in a way that maintains the structural strength simulated in this FEA, and because of the safety margin present in all of the simulated cases, a significant decrease in strength is not expected. However, other concerns about metal fatigue and simulation fidelity also exist. Since the aircraft will be expected to stay in service for a long time, loads under the yield strength can still cause catastrophic failure by propagating cracks to dangerous lengths. Theoretically, the larger the deformation is, the more likely it is for the wing material to fatigue and thus increase maintenance costs. Future considerations would address the expected lifetime and suggested maintenance intervals, but an in-depth analysis is out of the scope of this paper. We unfortunately did not have enough time to perform a fatigue analysis, but do want to acknowledge the importance of further analysis. If we were to delve into the details and provide an accurate estimate, we would need to either simulate millions of loading cycles in a software package or build the aircraft and test it. If we were to make preliminary guesses, we would use Basquin's Law and the Neuber correction for various ratios of these loading cases (Grover, 1966). We also note that we would add crack pathways by drilling holes when one initiates, use redundant structures, and design for a visible indication that a crack has begun that can be seen from the outside or when opening a maintenance panel. The basic static simulation in SolidWorks also has its own limitations because of the lack of wind flutters, gusts, and other dynamic perturbations. To help future developers improve the design, a lower aspect ratio wing ( $AR=9$ ) design was proposed and will be briefly discussed in the future work section as an alternative option.

## 7. Empennage

### 7.1 Design overview

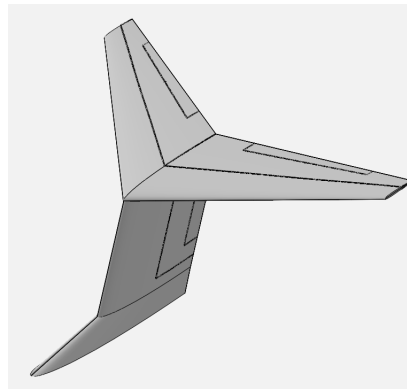
During the initial design phase for the aircraft, the team considered the advantages and disadvantages between the conventional, T-tail, and the H-tail designs. These design considerations are depicted in Table 7-1. Our trade study ranked stability as the most important aspect of the aircraft with weight, size, cost, and distance from airflow also considered as important. Stability was ranked as the most important aspect, because the aircraft will experience changes in weight throughout the flight as the payload is dropped. The empennage must adequately counteract the pitching moment produced by the wings throughout the Material Girl's flight and provide easy adjustments to the aircraft's orientation to keep it stable. After the trades were conducted, we decided that a T-tail would be the best choice for our final design. While we acknowledge the possibility of deep stall inherent in the choice of a T-tail, the only way to determine how it would affect our aircraft in high angles of attack would be through wind tunnel testing. We do not anticipate flying in such a scenario, but further studies could confirm whether deep stall is an issue and provide ways of addressing it. As seen in Table 7-1 below, the T-tail offered the most advantageous capabilities and was carried forwards in our design.

**Table 7-1.** Empennage Shape Trade Study

Design	Importance	Conventional	T-tail	H-tail
Stability	5	1	2	3
Weight	4	3	2	1
Size	2	2	3	1
Cost	1	3	1	2
Distance from Airflow	3	2	3	1
Total	-	30	34	26

In Figure 7-1, the shape of the empennage is shown. Both the horizontal and vertical stabilizers use the symmetric NACA-0010 airfoil. The empennage is very large because we wanted to integrate large control surfaces for maximum controllability. By increasing the size of the empennage, the aircraft would be able to generate larger

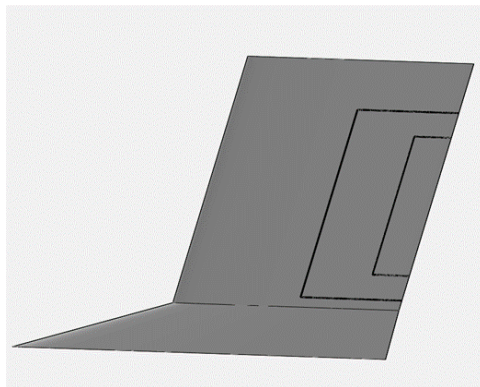
changes in pitch and yaw rates using the elevator and rudder. The T-tail also allows the aircraft to produce a natural upward pitch for takeoff and flight.



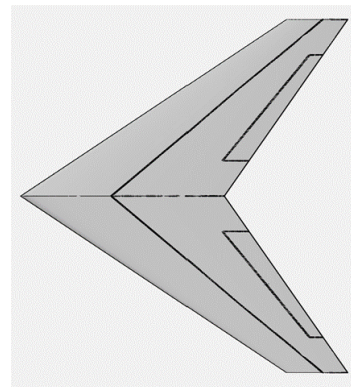
**Fig. 7-1.** Material Girl T-tail Empennage

## 7.2 Empennage Shape and Sizing

The Empennage is composed of both a vertical stabilizer and a horizontal stabilizer. Below, Figure 7-2 depicts the vertical component while Figure 7-3 shows the horizontal component of the tail. This section details the sizing process for these features.



**Fig. 7-2.** Material Girl Vertical Stabilizer



**Fig. 7-3.** Material Girl Horizontal Stabilizer

### Vertical Stabilizer

The Vertical Stabilizer is split into two different sections: a lower section and an upper section. Data on these sections are organized below in Table 7-2. The first, lower section of the tail has a high sweep angle to help separate the main tail from the fuselage. This section is used for structural integrity for the tail, similar to the design



of the Boeing 737. The second, upper section of the vertical tail is where the horizontal stabilizer is mounted. This section is relatively thick in order to maintain the structural integrity of the horizontal stabilizer. It has a sweep angle of 15 degrees inspired by the C-130 Hercules (Dickenson, 1953). The rudder and the trim tabs are also incorporated within this section. When sizing the vertical stabilizer, we used tail volume coefficients from similarly sized aircraft (Table 14, Nicolai et al.). We chose to model the sizing based off of current aircraft in service and future hypothetical aircraft undergoing testing including the SUGAR Volt (Bradley et al.). Comparative values of current aircraft are listed below in Table 7-3.

**Table 7-2.** Vertical Stabilizer Details

Parameter	Section 1	Section 2	Total
Span (ft)	5	27	32
Mean Aerodynamic Chord (ft)	26.5	20	23.25
Area (ft <sup>2</sup> )	132.5	540	672.5
Aspect Ratio	0.189	1.35	1.523
Sweep	60°	15°	—
Root Chord	33	20	—
Taper ratio	0.606	1	—

**Table 7-3.** Tail Volume Coefficients of Comparator Firefighting Aircraft

Aircraft	Vertical Tail Volume Coefficient
C-130	0.053
DC-10	0.060
Boeing 757	0.086
SUGAR Volt	0.687
Material Girl	0.0865

## Horizontal Stabilizer

Similar to the vertical stabilizer, the horizontal stabilizer used the same aircraft design texts (Nicolai et al.) and comparative aircraft to size. Most resources suggested that the sweep angle of the horizontal stabilizer should be 5 degrees more than the wing sweep, specifically for transport aircraft. To adhere to these suggestions, the horizontal stabilizers sweep was designed to have 41 degrees of sweep. To reduce the weight of the vertical stabilizer it is attached to, a twist angle of -5 degrees was included (Niu, 1988). Doing so reduces the torsional stiffness required and thus the thickness and weight. An incidence angle was also used to increase the stability and control of the aircraft. We tested different incidence angles from 0 to -10° and determined that the best angle was -7.5 degrees. This gave us the best trim angle during cruise. The optimization can be seen in Table 7-4.

**Table 7-4.** Trade Studies on Horizontal Tail Incidence Angle

Incidence Angle	Trim Angle of Attack
0°	1°
-2.5°	3°
-5°	6°
-7.5°	4.5°
-10°	7.25°

The overall span of the horizontal stabilizer is 60 feet, about a third of the span of the wing (Table 7-6). Similar to the vertical stabilizer, a larger configuration was desired when considering its size. The wide span allows the horizontal stabilizer to incorporate large control surfaces for generating larger pitch moments. The horizontal stabilizer's size was chosen to match the vertical stabilizer to maintain controllability and stability. The Material Girl's horizontal tail volume coefficient was also compared to similar aircraft, seen in Table 7-5 (Nicolai et al., Bradley et al.).

**Table 7-5.** Tail Volume Coefficients of Comparator Firefighting Aircraft

<b>Aircraft</b>	<b>Horizontal Tail Volume Coefficient</b>
<b>C-130</b>	0.94
<b>DC-10</b>	0.90
<b>Boeing 757</b>	1.15
<b>SUGAR Volt</b>	1.563
<b>Material Girl</b>	1.201

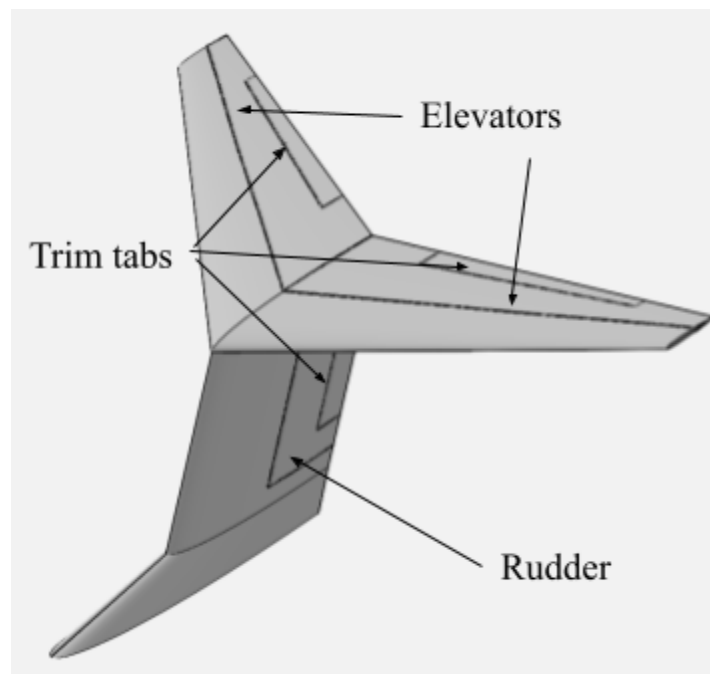
As can be seen above, the Material Girl's tail volume coefficient lies within the realm of similarly sized aircraft in operation and in testing. The dimensions of the horizontal stabilizer are given below in Table 7-6. Our rationale for the dimensions have been discussed above.

**Table 7-6.** Horizontal Stabilizer Details

<b>Vertical Stabilizer</b>	
<b>Parameter</b>	<b>Value</b>
<b>Span (ft)</b>	60
<b>MAC (ft)</b>	13
<b>Area (ft^2)</b>	780
<b>Aspect Ratio</b>	4.62
<b>Sweep</b>	41°
<b>Incidence</b>	-7.5°
<b>Twist</b>	-5°
<b>Root Chord</b>	20
<b>Taper ratio</b>	0.3

### 7.3 Control Surfaces

As with most traditional aircraft, the Material Girl incorporates a rudder, elevator, and trim tabs into the empennage design. All of the control surfaces were designed to be large and provide the most maneuverability. These control surfaces can be seen in Figure 7-4 below. The rudder dimensions are 45% of the chord length and make up 80% of total length of the vertical stabilizer's second section. The trim tabs dimensions are 16.5% of the chord length and span 57% of the upper section's length. The elevators and associated trim tabs are also designed to be large. The elevators extend the full span of the airfoil. They begin with 40% of the local chord at the wing tips and meet at the root with 55% of the local chord. The trim tabs extend 35% of the span of the horizontal stabilizer and use 15% of the local chord length. All of the control surfaces have a maximum deflection angle of 30 degrees upwards and downwards. These parameters were chosen in accordance with historical data and guidance from Raymer.

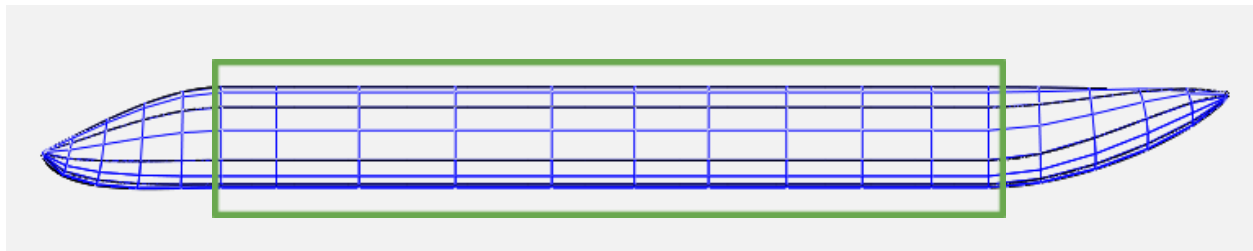


**Fig. 7-4.** Empennage control surfaces on Material Girl

## 8. Fuselage

### 8.1 Design overview

The Material Girl fuselage is 130ft in length with a near-circular body cross-section. The cargo area of the fuselage (boxed in green in Figure 8-1) spans 65% of the length, has a height of 10 ft and a maximum width at the bottom of 12 ft. This sizing was done to ensure the fuselage could fit the full cargo assembly with room for a drop mechanism (fire gates) and structural support. Since the fuselage must only carry the payload associated with firefighting (aside from small, emergency equipment), the payload deployment system comprises over 90% of the total length of the constant cross-section, or body, of the fuselage. The fuselage was determined to have near-zero lift capabilities due to its near-circular cross sections, which was verified using XFoil.0



**Fig. 8-1.** Fuselage left view. Cargo area shown by the green box.

### 8.2 Design approach

The design approach for the fuselage was primarily two-pronged, using OpenVSP and SolidWorks to iterate its design. In the initial conceptual mock-ups, other payload deployment aircraft inspired the team, like the C-130 Hercules shown in Figure 8-2. The notable borrowed design features of the C-130 include the use of a downswept contoured nose and a flat-bed payload drop area. These two features remained prominent throughout the design, despite their early addition to the fuselage. Once the contours and cross-section were chosen, the team briefly verified the near-zero lift capacity of the fuselage by running the coordinates of the constant cross-section through XFoil. Once it was determined that the cross-section did not produce large lift or downforce, the structure could then move to SolidWorks to focus on structural properties. Since the fuselage connects all of the aircraft components, any sizing change to the wings, empennage, or payload design would directly affect its size and shape,

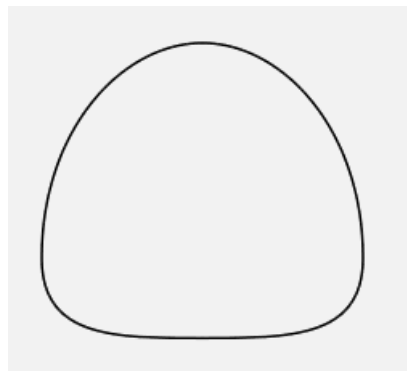
therefore sending the design back to OpenVSP to be iterated. In this way, the fuselage design drove the initial sizing of other components, but the later sizing changes would inevitably affect the fuselage's development.



**Fig. 8-2.** Lockheed C-130 Hercules. The Material Girl fuselage draws inspiration from its contoured nose and flat-bed fuselage.

### 8.3 General dimensions

The fuselage's shape is designed to support heavy, voluminous payload drops, to substantially fix each aircraft component with adequate strength, and to pressurize the vehicle during high cruise speeds. For payload housing, the fuselage was initially sized to exactly fit the payload, but this caused interferences with the wing fixing mechanism and fire gate system. Therefore, the height and width increased to 10 and 12 ft, respectively, to account for this. As a result of this, the outer skin of the fuselage increased in thickness from 0.08 to 0.1in to allow the fuselage to remain pressurized in flight without compressing in airflow. Figure 8-3 shows the constant cross-section of the fuselage and its flat-bottom shape.



**Fig. 8-3.** Fuselage payload area cross-section.

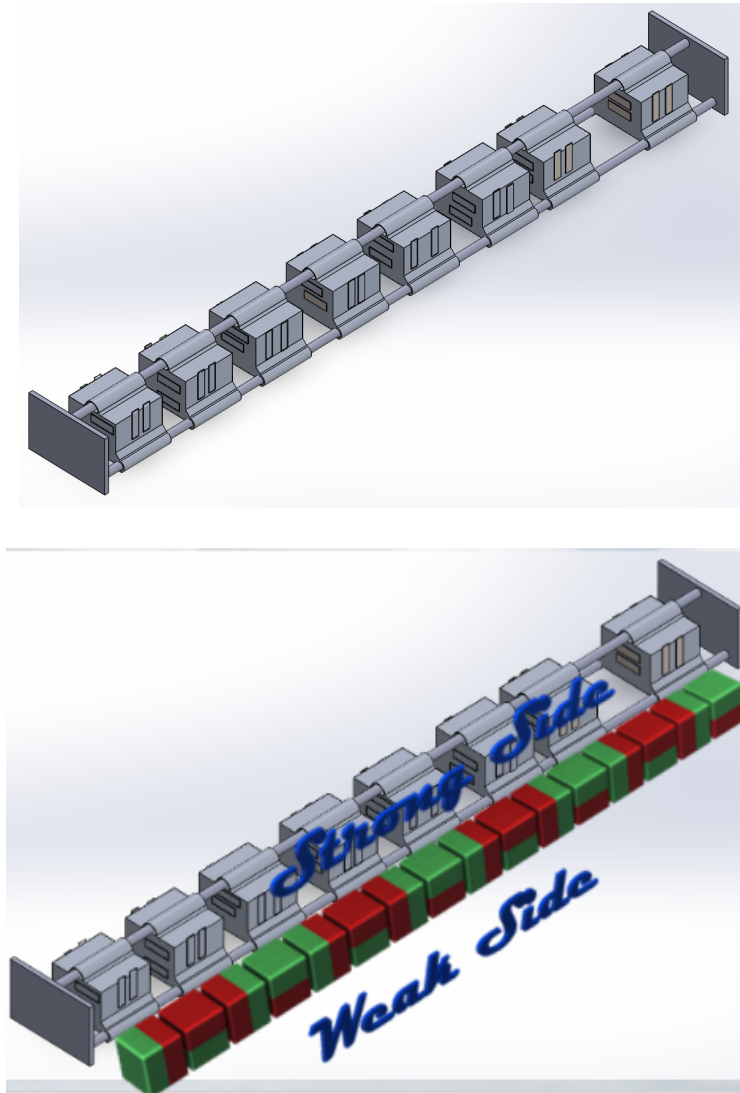
#### **8.4 Structural rigidity analysis**

The fuselage is supported internally by the endpoint walls of the payload system, as they are welded to the interior of the fuselage. In this way, the walls act as bulkheads, improving the bending and twisting moments that can be induced by the wings on the fuselage in flight. Additionally, the wall thickness of the fuselage was determined to be 0.1in based on the above analysis, and the prior value of 0.8in was found in comparing the outer fuselage wall to the Douglas Martin DC-10. To justify this wall thickness, the material composition of the outer skin is approximately 60% composites, 20% aluminum, 15% titanium, and 5% other metals, which is a higher composite percentage than other aircraft fuselages. This composition profile was selected with an emphasis on strength-to-weight ratio, in which state-of-the-art composites excel. The composites used in the Material Girl fuselage will be a cover layer of carbon fiber reinforced polymer (CFRP). To maintain manufacturability and sustainability requirements, the latest fabrication methods for both metals and composites will be used to minimize carbon emissions and cost.

#### **8.5 Payload Dropping Systems**

Carrying a large fluid payload on an air tanker is bound to create instability due to fluid sloshing and CG shifts once the mass is expelled onto the wildfire. Our team identified this as a key point for designing a payload system that would minimize potential for fluid slosh and CG shifts causing instability. This design is shown in Figure 8-4. It consists of eight compartments that can hold 1,000 gallons of payload each, capable of moving on a rail system to account for a moving CG. These compartments fit the payload when full without room for sloshing to occur. They have a compartment on the bottom which opens to dump the payload under the influence of gravity and the aircraft's acceleration alone. The rail system allows them to move along the flatbed of the fuselage where a larger payload bay opens by retracting along the sides of the fuselage during a drop. Our original payload design controlled the aircraft's CG through a system of magnets. Each individual payload compartment has an array of neodymium magnets on all 4 sides. These produce an eddy-current braking system between the containers to halt their movement after being slid along the rails by an external magnetic field (Pendrell et al., 2012). This magnetic field, drawing inspiration from the Inductrack permanent magnet maglev system, utilizes a Halbach array of magnets to provide the necessary force to move the heavy payload containers to the desired position (Bonsor et al., 2019) (Figure 8-4). Through these systems of permanent magnets and an external magnetic field generator, the

payload compartments could easily be moved to account for CG shifts during a payload drop. They would be repositioned to eliminate any permanent CG shift through a flight computer controlling the magnetic field before and after the drop.



**Fig. 8-4.** Payload system

Initially, we believed such a system would be necessary to reduce sloshing and large CG shifts. However, after conducting our weight analysis through FLOPS, the CG shift caused by dropping 4,000 gallons from the first four payload containers (the worst case scenario for CG shift), we found the CG only shifted by 0.17 ft. Thus, this complex system of controls was modified in favor of a simpler, yet still modular payload design.



To improve upon the prior design, the updated payload mechanism remains attached to a three-rod rail system, but is instead held in place by pin locks that are slotted through holes in each of the rails. Payload cells, pre-loaded with fire retardant, are loaded through the aft of the fuselage by debolting the aftward end plate and sliding the cells into position. The cells must be slotted in a mirrored configuration relative to the X coordinate of CG. Once each cell is in position, the payload is ready for takeoff and deployment. The primary benefit of this rail system is the simplicity and uniformity of the cells, which speeds up the “fueling time” by a massive margin, as the retardant is fueled and stored inside the cells prior to loading. The time of reloading depends on the competency of the loading crew, who is estimated to complete this task for full payload in a 15 minute time window, one minute below the RFP for 8,000 gallons of fuel. The payload system is modular such that it can be entirely replaced, allowing empty tanks to be refilled on the ground in between missions.

The bottom of each cell is equipped with an actuated electric door, which when activated, releases tension and allows the door to swing out, dropping the payload. In order for the retardant to leave the fuselage, there is a fire gate installed in the bottom of the fuselage, spanning the length of the rail system. To remove the payload cells, the fuselage aft opens up, the aft end plate is debolted, and the cells slide out once the pin locks are removed.

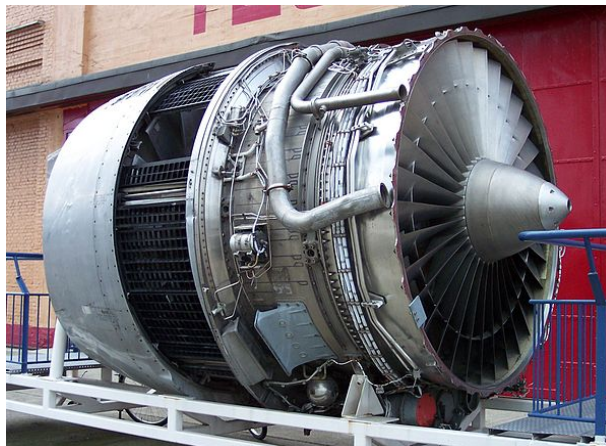
## 9. Propulsion

### 9.1 Design overview

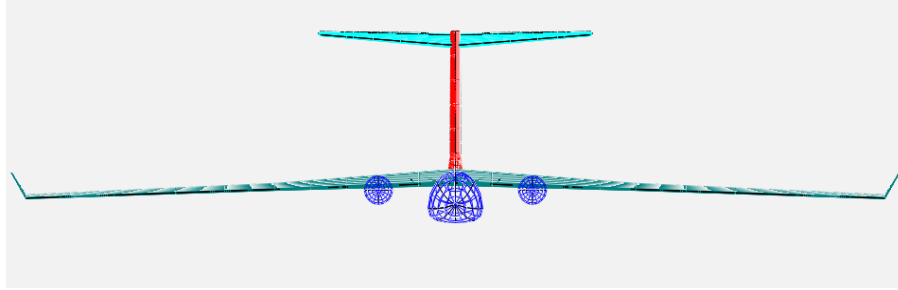
The engine that was chosen for Material Girl was a Rolls-Royce RB211 (Figure 9-1) which is a triple-spool high bypass turbofan. Seen below in Table 9-1 are the characteristics of this engine.

**Table 9-1.** Engine Characteristics

<b>Series</b>	-535
<b>Length</b>	198.2 in
<b>Diameter</b>	86.3 in
<b>Dry Weight</b>	8170 lb
<b>Compressor</b>	1 Fan, 6 IP, 6 HP
<b>Combustor</b>	Annular
<b>Turbine</b>	1 HP stage, 1 IP stage, 3 LP stage
<b>Max Net Thrust</b>	42500 lbf
<b>Bypass Ratio</b>	4.4:1
<b>Maximum continuous Thrust TSFC (sea level)</b>	5.21
<b>100% RPM</b>	HP 10611, IP 7000, LP 4500



**Fig. 9-1.** Engine used on the Material Girl. Two Rolls-Royce RB211 engines on Material Girl. They are located 17 ft from the center line as shown by Figure 9-2.



**Fig. 9-2** Front View: Depicting engine integration

## 9.2 Design approach

In order to analyze this, the engine and its capabilities and produce values necessary to develop and engine deck and add them to FLOPS, GasTurb was used. A mixed flow, three spool, high bypass ratio, turbofan was selected and the input data was altered to fit Material Girl's specific engine customizations. This analysis was done over an altitude range (alt) of 0-25,000 ft, in 1,000 ft increments, and 0-0.8 for Mach (XM) in increments of 0.1 (which are the inputs in Fig. 9-3). The output of the gross thrust (FG), fuel flow (WF), NOx emissions index (sNOx), and nozzle exit area (A8) with their corresponding altitude (alt) and flight Mach number (XM) are attached below in Figure 9-3:

alt	XM	FG	WF	sNOx	A8
0	0	44275	4.0421	1.1375	1555.5
3280.8	0	40275	3.6887	0.9934	1531.6
6561.7	0	36394	3.3568	0.86617	1519.7
9842.5	0	32735	3.0464	0.75313	1513.8
13123	0	29328	2.7561	0.65394	1511.6
16404	0	26178	2.4855	0.56696	1512.1
19685	0	23282	2.2339	0.49079	1514.7
22966	0	20631	2.0008	0.42418	1519
26247	0	18212	1.7858	0.36564	1524.8
29528	0	16015	1.588	0.3143	1532.1
32808	0	14026	1.4063	0.26966	1540.8
36089	0	12231	1.2402	0.23092	1550.8
39370	0	10446	1.0593	0.2168	1551.3
42651	0	8921.2	0.9048	0.20355	1551.9
45932	0	7618.8	0.77284	0.19111	1552.5
49213	0	6506.4	0.66013	0.17943	1553.2
52493	0	5556.3	0.56385	0.16846	1554
55774	0	4744.7	0.48162	0.15816	1554.9
59055	0	4051.5	0.41138	0.14849	1556.1
62336	0	3459.3	0.35138	0.13942	1557.4
65617	0	2953.7	0.30014	0.13089	1558.8
68898	0	2521.6	0.25637	0.12289	1560.7
72178	0	2152.7	0.21899	0.11538	1562.7
75459	0	1837.5	0.18706	0.10833	1565.3
78740	0	1568.3	0.15979	0.10171	1568.2
82021	0	1338.3	0.13649	0.095489	1571.6
0	0.1	44633	4.0602	1.1495	1558.6

**Fig. 9-3.** Engine gross thrust, fuel flow, NOx index, and nozzle exit area at specific altitude and flight speed.

## **10. Avionics, Technology, and Subsystems (Auxiliary Systems)**

### **10.1 Flight Controls**

All of the control surfaces will be powered by an electric system powered by the engines on the aircraft. Currently, the main flight control systems include the elevator, rudder, ailerons and any other flaps. Whether to equip more systems will depend on if we are going to add a fly by wire system to assist the pilot in flight and how to effectively implement it. Further research will need to be conducted in order to determine how autonomous features of the aircraft will help control the flight controls.

### **10.2 Subsystems**

Due to the civilian use status of this aircraft, Instrument Flight Rules (IFR) and Visual Flight Rules (VFR) must be met. In order to abide by these requirements, the aircraft is expected to have equipment to allow the aircraft to be flown under instrument meteorological conditions (IMC).

Equipment that satisfy IFR include:

- Two-way radio communication and navigation equipment
- Gyroscopic rate-of-turn indicator
- Slip-skid indicator
- Sensitive altimeter adjustable for barometric pressure
- Clock
- Generator
- Gyroscopic pitch, bank, direction indicator

Equipment that satisfy VFR include:

- Airspeed indicator
- Altimeter
- Magnetic direction indicator
- Tachometers for each engine
- Oil pressure gauges for each engine

- Fuel gauges
- Landing gear position indicator
- Approved position lights
- Electric landing light
- Approved aviation red anti-collision light system

### **10.3 Electrical System**

There are two AC generators providing power to the entire electrical system of the Material Girl. Power is mainly used to power each of the turbofan engines providing the thrust. Aside from powering the two engines, electricity is then routed to power flight control actuators that control flaps on both the wing and tail. In addition to this, lower power electronics like cockpit instruments and displays are also accounted for.

### **10.4 De-ice and Anti-icing Systems**

To protect aerodynamic surfaces from ice formation and accumulation, an anti-ice system is implemented using state-of-the-art technologies. To prevent ice formation on the wing and horizontal tail leading edges, an electrothermal anti-icing system will be employed, using thermal coils under the skin to maintain a high-temperature surface during flight. The entire system is split into three primary areas: left wing, right wing, and horizontal tail. Each electrothermal subsystem is routed into the same central AC generator system described above, using a modest amount of power in-flight.

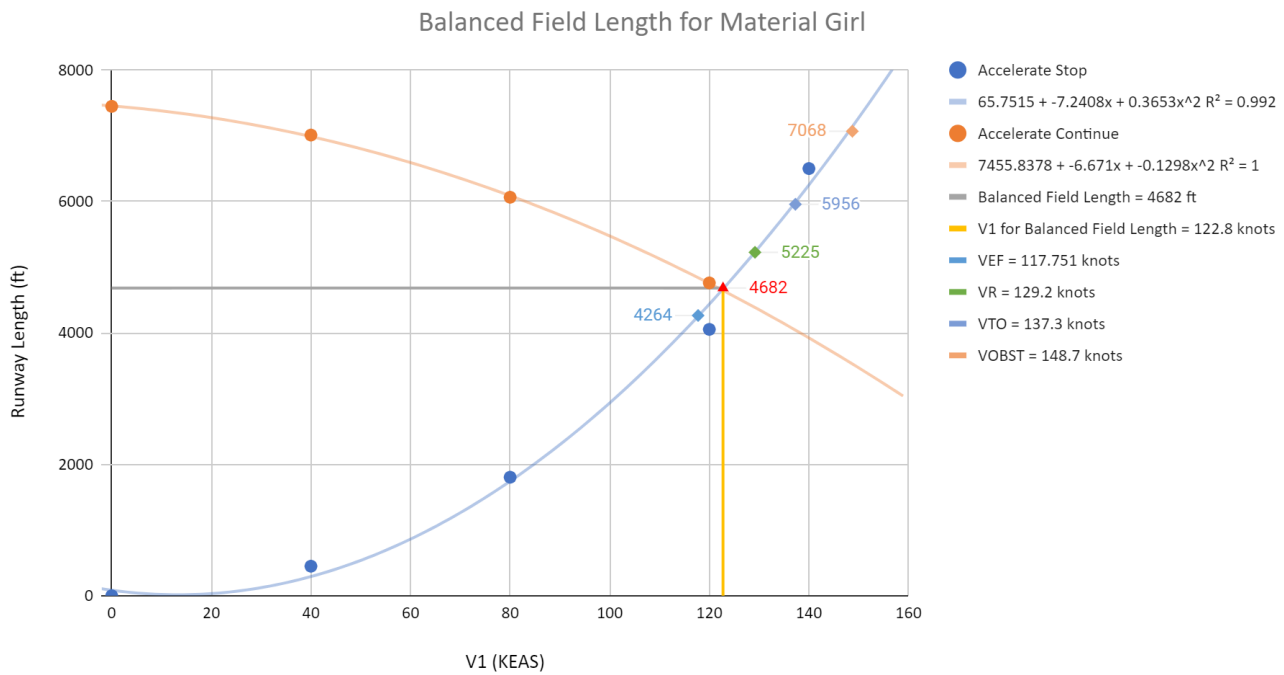
On non-lifting surfaces, like the fuselage, engine nacelle, and vertical tail, a hydrophobic coating system named “SLIPS”, or Slippery Liquid Infused Porous Surfaces, will cover the entire surface area. These coatings use the combination of a very porous material and a nonpolar liquid acting as a lubricant to lower the friction coefficient on the surfaces, preventing water from sticking and forming ice. Though this is less effective in-flight than other anti-icing methods, SLIPS is especially effective in off-season ice prevention, when ice could accumulate on the airplane while being stored in a hangar. Since the coating is so inexpensive, the recommendation is to use the coating in storage and reapply for flight missions.

## 11. Performance Analysis

### 11.1 Takeoff & Landing

To ensure our aircraft met the balanced field length requirements stipulated in the RFP, we wanted to minimize the takeoff weight, while maximizing engine thrust and lift. Comparing our aircraft design with the field performance of the B757, we anticipated that this aircraft is likely able to meet the 8,000 ft balanced field length requirement. Our plane has an MTOW that is slightly lower than that of the B757 series, and it is designed to use the nominal landing gear system of Boeing commercial aircraft. B757 has a balanced field length of 6920 ft. Rolls Royce RB211 turbofan engines are used on the B757; this is the same engine selection for Material Girl. Therefore, the engine thrust on both aircraft will be similar, resulting in comparable performance results which impact the balanced field length. Due to the reasons above, we expect that our aircraft will likely have a similar balanced field length. Other components that influence balanced field length include airport elevation and the presence of precipitation or ice. Precipitation and icing cannot be planned for, and it is likely that Material Girl will take off on landing strips at high elevation. Due to this, the goal was to minimize the balanced field length to accommodate for unplanned situations. By matching the aircraft's characteristics to that of a B757, that goal was easily achieved.

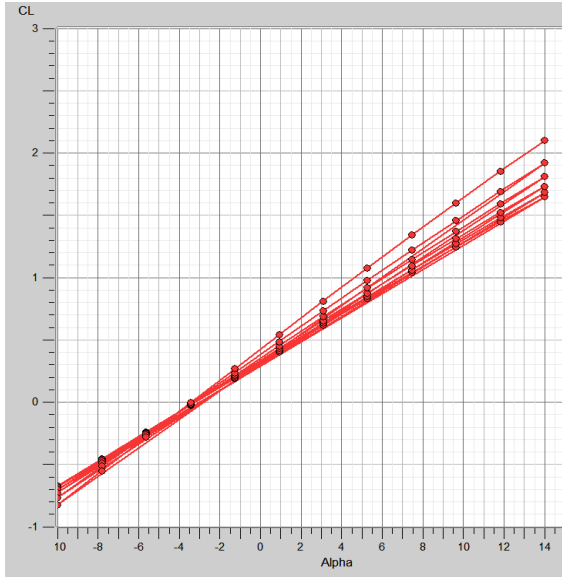
Per the FAA Part 25 regulations, the aircraft must reach a decision speed  $V_1$  before the pilot decides to reject or continue the takeoff. At this point, two scenarios can occur. If engine failure occurs up to 1 second before reaching this speed, at  $V_{EF}$ , the takeoff will be rejected and the brakes will be applied to stop the aircraft before the end of the runway, known as Accelerate-Stop. Otherwise the pilot will continue taking off with the one remaining engine, known as Accelerate-Continue. Using the methods from Nicolai et al. (2010) and Schaefe (2007), curves of these two scenarios were determined and plotted on Figure 11-1. All calculations assumed an elevation of 5,000 ft above mean sea level (MSL) on a +35°F hot day. Calculations up to and including  $V_{EF}$  assumed all engines were operable (AEO), while rotation speed ( $V_R$ ), takeoff speed ( $V_{TO}$ ), and obstacle speed ( $V_{Obst}$ ) were calculated with one engine inoperable (OEI). These speeds, along with the location on the runway they are achieved, are shown in Figure 11-1. After performing these calculations and finding the intersection of the two curves,  $V_1$  was determined to be 122.8 knots with a balanced field length of 4682 ft (Figure 11-1, red triangle). This falls below the objective of the 5000 ft stipulated in the RFP.



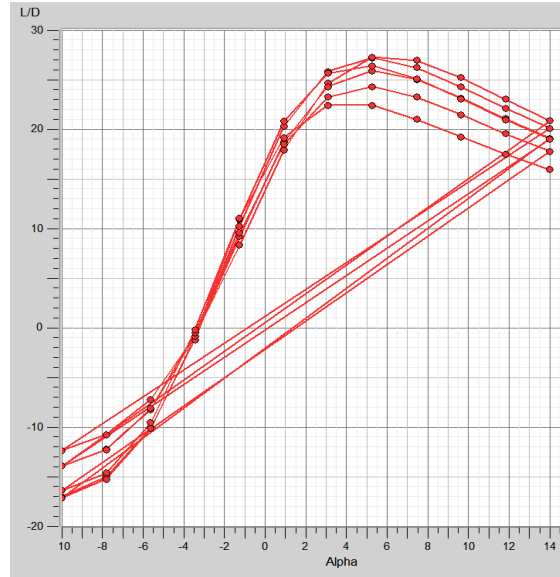
**Fig. 11-1. Balanced Field Length**

## 11.2 Cruise

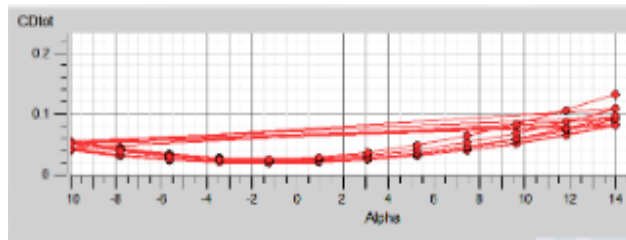
Using VSPAERO, we determined the coefficient of lift, drag, and lift-to-drag ratio from  $-10^\circ$  –  $14^\circ$  angle of attack over a Mach number range of 0.2–0.8. This data helped us determine the optimal angle of attack to fly at for the best performance. As can be seen in Figure 11-2, 11-3, & 11-4 flying at the trim angle of  $4.5^\circ$  gives us the best lift-to-drag ratio, and thus improves our fuel efficiency during the mission.



**Fig. 11-2.** Coefficient of Lift vs Angle of Attack



**Fig. 11-3.** Lift-to-drag ratio vs Angle of Attack



**Fig. 11-4.** Coefficient of Drag vs Angle of Attack

### 11.3 Range & Endurance

Full payload mission radius is 400 nmi. As shown in Figure 11-5, this aircraft can easily cover the entire state of California on firefighting missions if based in SFO or LAX airports. For most other states, the aircraft can also cover the entire area as long as it is based in a medium to large hub airport.





**Fig. 11-5.** Full-payload mission coverage from major airports in California.

The ferry mission range is 2,000 nmi. As shown in Figure 11-6, our aircraft is able to meet the RFP requirement to transport to remote locations for international firefighting missions or rentals. This capability makes our design more competitive over some current air tankers because it can be easily flown to other countries to participate in more wildfire suppressions.



**Fig. 11-6.** Ferry mission coverage from major wildfire-prone cities around the world.

## 11.4 Stability and Control

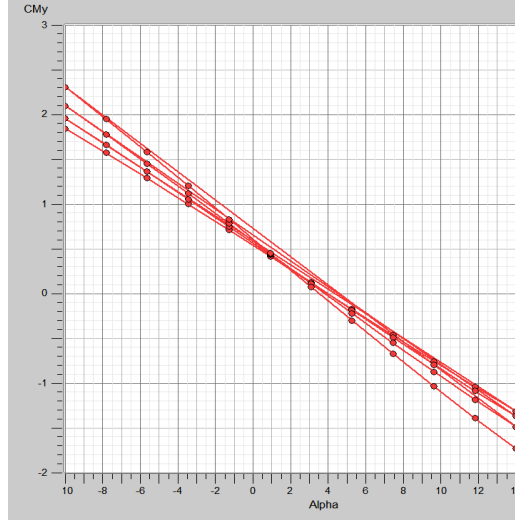
The Material Girl is an air tanker class aircraft designed for high maneuverability. The high-mounted anhedral wings serve to not only provide visibility for the pilot and adequate ground and obstacle clearance, but make it easier for the aircraft to roll and maneuver through tight terrains while completing low and slow payload drops. Despite being designed for high maneuverability, it must still be statically stable and controllable to be effective at responding to wildfires.

## 11.5 Longitudinal Static Stability

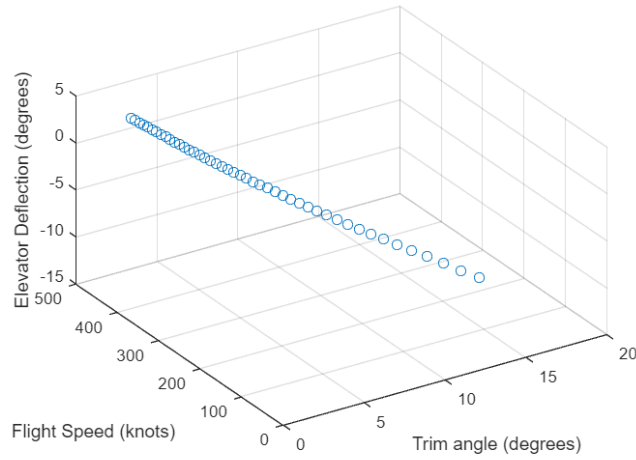
Determining whether Material Girl is longitudinally stable is essential to prevent unrecoverable nose-up or nose-down pitching during turbulence. To calculate the longitudinal stability characteristics, a stability analysis was conducted in VSPAERO sweeping from  $-10^\circ$  to  $14^\circ$  angle of attack and a Mach number of  $0.2 - 0.8$ . The pitching stability derivative as well as trim angle are summarized in Table 11-1 below, and a visual depiction of the trim angle range over the design and ferry missions can be seen in Figure 11-7 & 11-8. From this analysis, we can conclude that our aircraft is statically stable in pitch due to a negative  $Cm_\alpha$  and positive  $\alpha_{trim}$ . The coefficient of lift at this trim angle of attack is sufficient to keep our aircraft airborne in steady, level flight.

**Table 11-1.** Longitudinal Stability Characteristics

Parameter	Value
$Cm_\alpha$	-7.56
$Cm_0$	0.6
$\alpha_{trim}$	$4.5^\circ$
$CL_{\alpha_{trim}}$	0.8



**Fig. 11-7.** Plot of Pitch Moment vs Alpha over mission



**Fig. 11-8.** Elevator deflection – flight speed – trim angle space during mission

We wanted our aircraft's trim angle to be between  $3^\circ$  and  $6^\circ$  to prevent a need for constant deflection of the elevator to achieve steady flight. We did not want the trim angle of attack to deviate from this range so the coefficient of lift would be sufficient to maintain flight while also avoiding stall or dropping off significantly when turbulence is encountered. Using methods from Nelson (1998), equations 7-10 were used to calculate the necessary deflection of the elevator to maintain trimmed flight throughout the design and ferry missions. From the VSPAERO output, the trim angle of attack ranged from  $3.75^\circ - 5^\circ$  and the elevator would need to be deflected  $1.09^\circ - -0.62^\circ$  over this range, which can easily be accomplished through trim tabs.

$$\delta_e = (Cm_0 + C_{m_{\alpha_{trim}}})/V_H C_{L\delta_e} \quad \text{Eqs. (7)}$$

$$V_H = l_t S_t / S \bar{c} \quad \text{Eqs. (8)}$$

$$\alpha_{trim} = C_L / C_{L\alpha} \quad \text{Eqs. (9)}$$

$$C_L = W / (0.5 \rho V^2 S) \quad \text{Eqs. (10)}$$

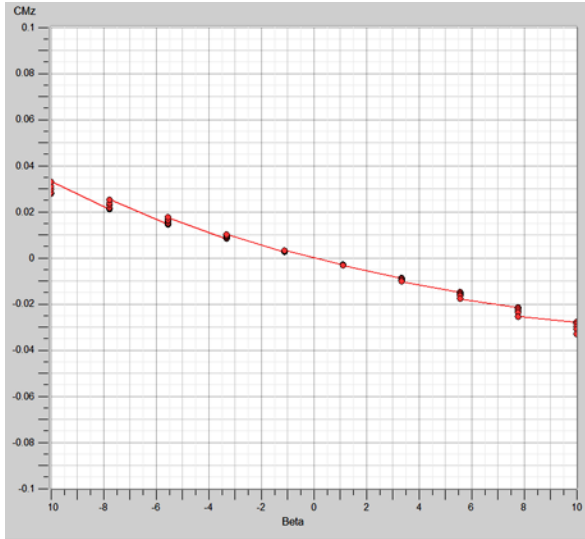
Where  $\delta_e$  is the elevator deflection,  $Cm_\alpha$  is the longitudinal stability derivative,  $V_H$  is the horizontal tail volume coefficient,  $l_t$  is the distance between the aerodynamic center of the horizontal stabilizer and the CG,  $\bar{c}$  is the mean aerodynamic chord of the wing,  $S_t/S$  is the ratio of horizontal tail area to wing area,  $C_{L\alpha}$ ,  $C_{L\delta_e}$  are the lift curve slopes of the wing and horizontal stabilizer (respectively),  $Cm_0$ ,  $\alpha_{trim}$  are the intersection of the pitching moment curve with the vertical and horizontal axis seen in Figure 11-7 (respectively),  $C_L$  is the coefficient of lift,  $W$  is the maximum takeoff gross weight,  $\rho$  is the air density, and  $V$  is the air speed.

## 11.6 Lateral and Directional Static Stability

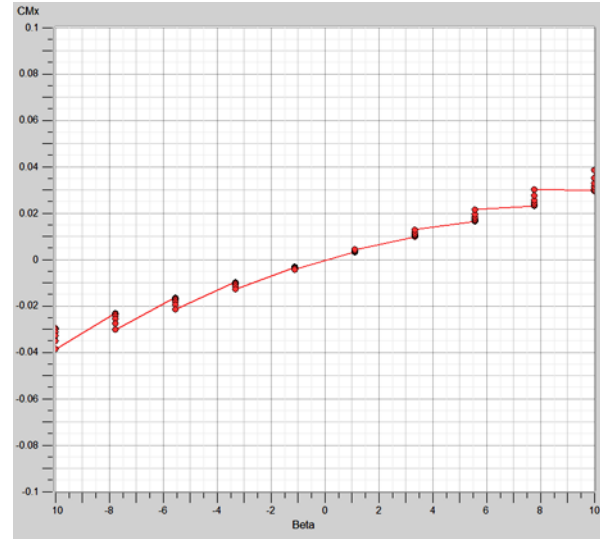
Lateral and Directional stability is important to prevent spiraling and Dutch Rolls for the Material Girl in unsteady flight. To determine our aircraft's stability characteristics in these axes, VSPAERO was used to sweep from  $-10^\circ - 10^\circ$  sideslip angle over a Mach range of 0.2 – 0.8 at the trim angle of attack for the respective flight speed. The results of this analysis can be seen in Table 11-2, and Figures 11-9 and 11-10 below. The roll stability derivative is positive, which shows that given a sideslip disturbance, the tendency of the aircraft is to roll back to neutral with a restoring moment. Similarly, the negative yawing stability derivative means that the Material Girl will produce a restoring moment around the yawing axis under a sideslip disturbance. The magnitude of the roll stability derivative is greater than that of the yaw, so spiraling instability will be avoided.

**Table 11-2.** Lateral and Directional Stability Derivatives

Derivative	$Cl$	$Cn$
Value	0.232	-0.141



**Fig. 11-9.** Plot of Roll moment vs Sideslip



**Fig. 11-10.** Plot of Yaw moment vs Sideslip

### 11.7 Dynamic Stability

Static stability is essential for steady flight, but the Material Girl must also be dynamically stable so that phugoid and short period modes of oscillation do not grow without bound and make the aircraft unrecoverable. This is especially important in the low-visibility environments often prevalent when responding to wildfires. If one of these modes were to become unstable, the aircraft responding to the fire is at risk of not only impacting other aircraft at the scene, but also obstacles on the ground due to the low drop altitudes and mountainous, densely-forested terrain. Thus, ensuring the Material Girl meets the conditions of dynamic stability was essential for it to be effective at fighting wildfires. A dynamic stability analysis was conducted through VSPAERO with its unsteady simulation tools. The results of this analysis are shown in Table 11-3.

**Table 11-3.** Dynamic Stability Derivatives

Derivative	$Cl_p$	$Cn_p$	$Cl_q$	$Cm_q$	$Cl_r$	$Cn_r$
Value	-0.537	-0.180	29.5	-159.4	0.773	-0.170

The relationships and signs of  $Cl_p$ ,  $Cn_p$ ,  $Cl_q$ ,  $Cm_q$ ,  $Cl_r$ , and  $Cn_r$  are in agreement with the values from the Boeing 747 in a report by Heffley et al., an aircraft nearly twice as heavy as the Material Girl, but nonetheless similar in size. Also,  $1/3 < |Cn_p/Cl_p| < 2/3$ , which ensures that the Material Girl will be recoverable from both Spiral and Dutch Roll modes of dynamic instability according to Brandt et al (2004). Therefore, we concluded that

because the dynamic stability derivatives for the Material Girl align with similar aircraft and satisfy Brandt et al.'s criteria for avoiding Spiraling and Dutch Roll, our aircraft is dynamically stable. Further analysis could potentially determine how inertial coupling plays a role in the Material Girl's dynamic stability, but this was deemed out of scope for the conceptual design phase. Accounting for this would be left to a systems integration analysis and most likely be regulated by a flight computer.

## 11.8 CG and Static Margin

The location of the Material Girl's Center of Gravity (CG) is important not only for static stability, but also due to the fact it is carrying a heavy fluid payload on board. This, as well as fuel, will be expended by the end of the mission. The shifts in CG, and consequently the static margin, caused by loss of weight must be accounted for in order to ensure stable flight over the entire mission. To determine the location of the CG at various points during the mission, equation 11 was used.

$$X_{CG} = \frac{\sum_i^n \bar{X}_i * W_i}{\sum_i^n W_i} \quad \text{Eqs. (11)}$$

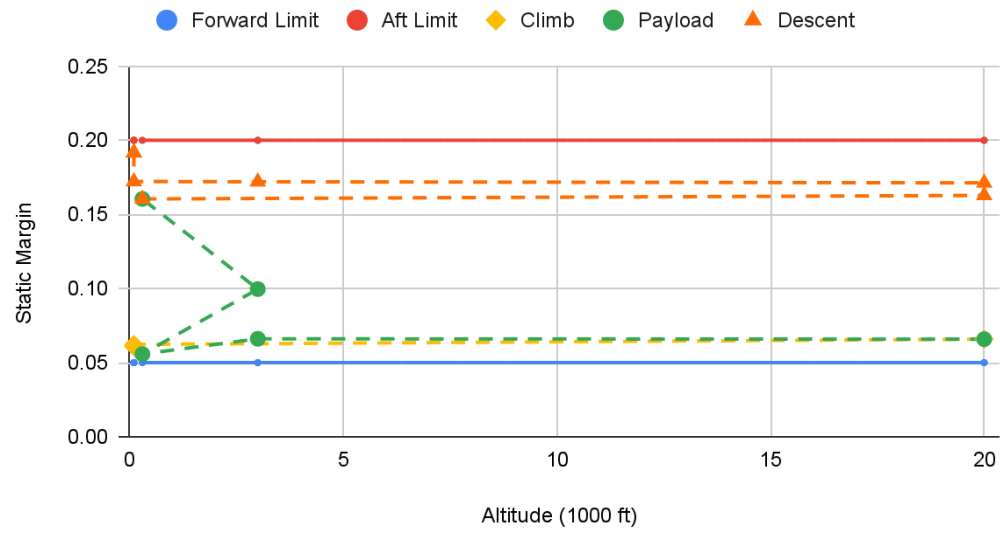
The weights of each component were determined through FLOPS, and the location of each component's CG was assumed to be the geometric centroid due to uniform density throughout the entire component. Further analysis could determine a more precise location given the possibility of composite materials and minor flaws during the manufacturing process, but we do not expect it to deviate significantly from our estimation. The center of mass with full payload and fuel is given in Table 11-4 below.

**Table 11-4.** CG Location During Design and Ferry Mission

	<b>Design</b>	<b>Ferry</b>
<b>Segment</b>	<b>CG location</b>	
<b>Full</b>	70.69	70.69
<b>Taxi</b>	70.68	70.68
<b>Takeoff</b>	70.68	70.68
<b>Climb</b>	70.66	70.66
<b>Cruise</b>	70.60	70.60
<b>Cruise</b>	70.60	70.60
<b>Drop Payload 1*</b>	70.77	70.60
<b>Cruise</b>	70.03	70.60
<b>Drop Payload 2*</b>	69.01	70.60
<b>Climb</b>	68.97	70.58
<b>Cruise</b>	68.83	70.54
<b>Descent</b>	68.81	70.54
<b>Approach</b>	68.81	70.54
<b>Reserve</b>	68.48	70.45
<b>Taxi</b>	68.48	70.45
= Climb Segment, = Payload Segment * only for design mission, = Descent Segment		

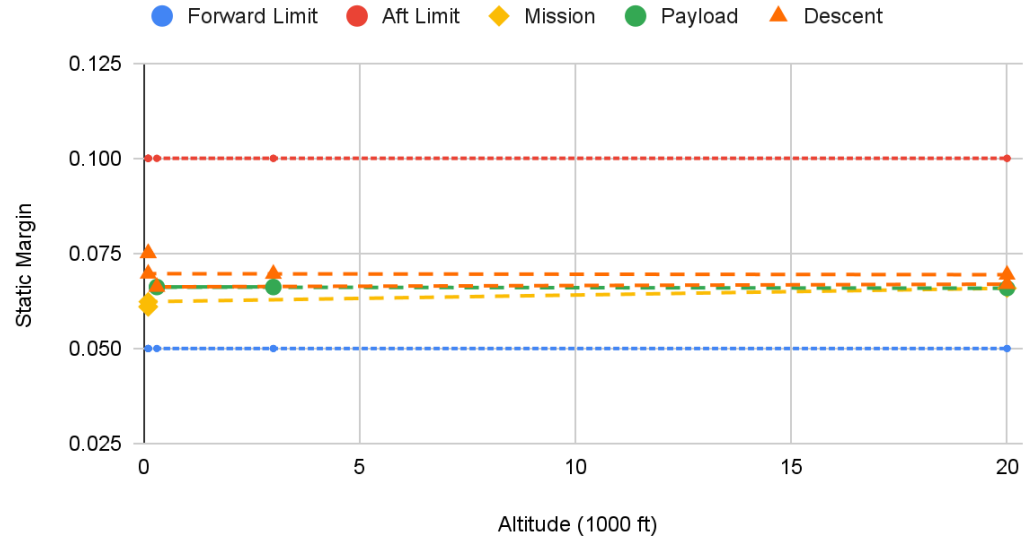
As the mission progresses, the CG will move when fuel is burned. To account for this, the fuel is stored in the wings, and the payload is centered at the CG's location excluding it. The CG travel over the design and ferry missions can be seen in Table 11-4. In the design mission, we simulated multiple payload drops in our calculation of the CG. Since the CG only shifted aft by 0.17 feet after a payload drop, the self-adjusting payload system shown previously was deemed unnecessary (further justification of design change discussed previously as well). We configured our aircraft so that once the payload was dropped and the fuel was burned, it would become more statically stable. The CG moving forwards while the neutral point stayed fixed (due to no changes in wing geometry) is evidence of this. A visual depiction of the static margin of the Material Girl over the design and ferry missions are shown in Figures 11-11 & 11-12 below. The location of the CG and neutral point with full payload is given in Table 11-5 and Figure 11-13.

### Static Margin Range Design Mission



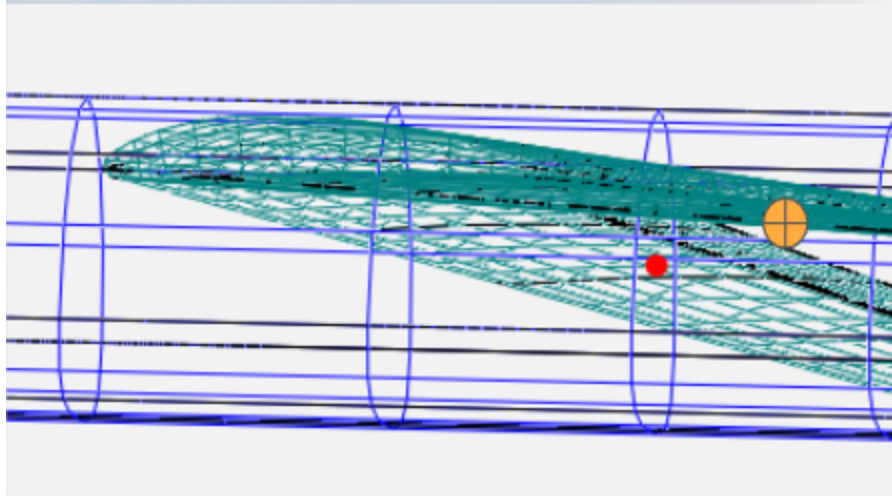
**Fig. 11-11.** Static margin over design mission

### Static Margin Range Ferry Mission



**Fig. 11-12.** Static margin over ferry mission





**Fig. 11-13.** CG location (red dot) and neutral point (orange cross)

**Table 11-5.** Neutral Point and CG Location

	<b>X position (from nose) [ft]</b>	<b>Y position (from fuselage centerline) [ft]</b>	<b>Z position (above fuselage centerline) [ft]</b>
<b>CG</b>	70.68	0	2.3
<b>Neutral Point</b>	71.71	0	3.35

The forwards and aft limits for the static margin were chosen in accordance with guidance from Raymer and historical aircraft data. The design mission had a wider tolerance for increase in static margin due to the fluid payload, and because the Material Girl had to be more maneuverable in the earlier parts of the design mission than the ferry mission. Even with this goal in mind, it would have been preferable to stay within the narrower static margin range (5% – 10%) for both the design and ferry missions. The fact that the static margin varied outside this typical range supports the need for our theoretical moving payload deployment system. However, due to the associated cost of maintenance we would expect for such a system, this would be left as an optional feature for the consumer. They would need to decide based on whether they prioritize a narrower static margin and higher costs, or are satisfied with the wider range and fluid slosh.

## **12. Cost Analysis**

### **12.1 Stakeholders and Market Analysis**

Existing stakeholders largely consist of fire departments with large budgets. CAL FIRE, California's fire department, utilizes numerous air tankers to combat increasingly damaging wildfires. CAL FIRE receives an estimated budget of \$3.7 billion in total for 2021-22, increasing from only \$800 million in 2005-2006. In addition to CAL FIRE, Fire and Rescue NSW, an Australian fire department located in New South Wales, is expected to have an annual budget of \$1.9 billion. These fire departments have fleets that combat bushfires and forest fires and have been known to require the use of larger air tankers in order to efficiently lay down fire retardant where needed.

Other stakeholders are manufacturers of the plane. Notable manufacturers and engineering firms like Boeing and Lockheed Martin are capable of producing military aircraft that may similarly resemble the performance attributes of our air tanker. These manufacturers will be able to produce and possibly lease the aircraft to various fire departments around the world or sell the plane to companies wishing to lease it themselves. Companies like 10 Tanker are known for their renovated DC-10 air tankers and charge fire departments to utilize their services during wildfire seasons as their business model.

Direct competitors to this proposed aircraft include any Very Large Air Tanker (VLAT). This includes the DC-10 and the Boeing 747, both of which can hold 11,600 gallons and 17,500 gallons, respectively. The DC-10 costs \$55,700 per drop while having an hourly fee of \$8,200. The Boeing 747 has an estimated cost of \$65,000 per drop. Both are marketed as a cheaper alternative than using smaller air tankers due to their ability to drop large retardant loads when necessary. When compared to the cost estimates for this proposed aircraft, this aircraft remains competitive when compared to the current and active VLATs.

### **12.2 Cost analysis of the final design**

Cost for the Material Girl was calculated utilizing the Advanced Aircraft Analysis (AAA) software, specifically its cost calculator. The AAA software is based upon the textbook *Airplane Design* by Dr. Jan Roskam, and allows for the adjustment of inflation to ensure cost accuracy. The software utilizes input factors like take-off gross weight, propulsion costs, and program manufacturing figures to fully utilize the equations taken from the textbook. As seen in Figure 12-1, AAA utilizes equations within the software to predict and return expected

numbers for costs. Cost analysis involves research and development as well as manufacturing phases. As for research and development, major factors inputted into AAA include the takeoff gross weight, expected number of planes produced during research and development, and the expected year of entry of service of 2030. As calculated by AAA, the total engineering man hours were predicted to be over 1.5 million to properly design the plane. In addition to this, \$197 million is expected to be the research cost for this particular airplane.

The manufacturing phase is then calculated with an expected cost of \$95 million. A single aircraft acquisition cost is expected to be \$290 million. Avionics within each manufactured plane is \$7.5 million, while the RBS211 engines cost \$3.5 million each. This stems from a manufacturing program of 10 total aircraft and pricing in regards to expected man hours during both manufacturing and research and development.

Input Parameters							
$C_{aed\_man}$	95.266	$10^6 \$$	$C_{tto\_man}$	4.982	$10^6 \$$	$F_{fin\_man}$	0.20
$C_{prod\_man}$	901.289	$10^6 \$$	$F_{pro\_man}$	0.10	$C_{rdte}$	1195.358	$10^6 \$$
						$N_{man}$	10
Output Parameters							
$C_{pro}$	125.192	$10^6 \$$	$C_{man}$	1251.922	$10^6 \$$	$P_{ap\_est}$	257.247
$C_{fin\_man}$	250.384	$10^6 \$$	$C_{acq}$	1377.115	$10^6 \$$		

**Fig. 12-1.** Screenshot of the AAA user interface on the “Total Cost” window

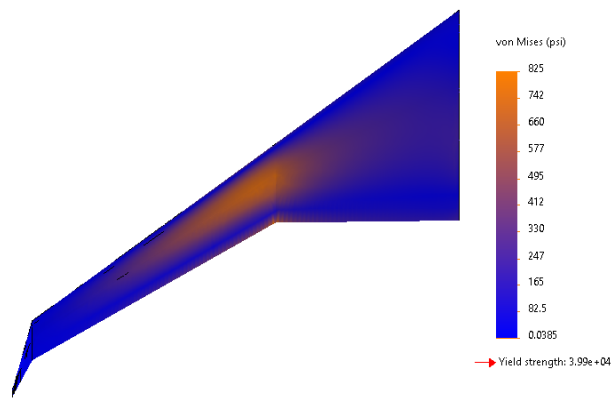
Our mission profile expects the plane to operate around 3 hours at a time. Through AAA, we calculated that the flight operation per hour is around \$12,240; this does not include the retardant. The retardant used is Phos Chek LC95 that costs \$2.50 per gallon. With 8,000 gallons used per mission, there is an additional \$20,000 added for retardant costs, and the total mission cost over three hours is expected to be \$56,720. The assumptions of a two man crew to operate the aircraft and 1200 flight hours per year were made and integrated as input within the software to calculate the flight operation per hour. This would be the total mission cost considered when proposing contracts to potential fire departments and air tanker companies. AAA predicts the total production program cost to be \$2.1 billion, which is most likely attributed to the complexity of the aircraft and its state-of-the-art focus on firefighting in addition to designing, researching, and manufacturing a plane completely from scratch. This is different from current air tankers that are remodeled military and civilian aircraft, which makes them a cheaper alternative. To reach 15%

profitability, each plane must be sold at around \$210 million considering the entire program cost and with an initial production fleet of 10 aircraft.

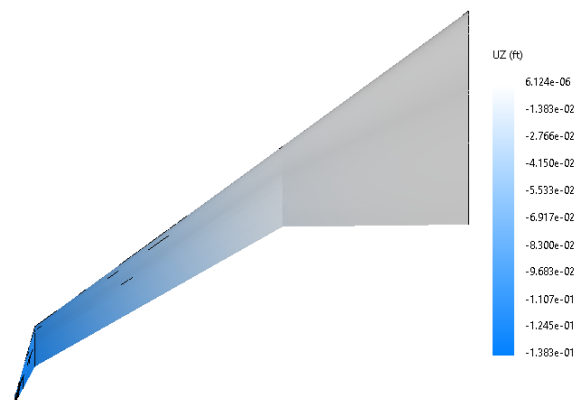
Research and development along with manufacturing costs will decrease significantly after the first year due to less of a need of initial investment. The US Forest Service spent an average of \$2 billion over the past five years in order to suppress wildfires. The Office of Wildland Fire within the US was appropriated \$1.53 billion for the 2022 Wildland Fire Management Budget. That allows a steady market in the US alone to spend on potential companies owning the Material Girl similar to the 10 Tanker's DC-10. The intensifying wildfires have incentivized firefighting departments to spend more on retardant drops to prevent even more expensive damage to both forests and properties. With manufacturing costs to decrease after the initial manufacturing year and an increasing demand for air tankers, the airplane will be able to remain profitable to manufacture and even develop when needed.

### **13. Next Steps**

The first suggestion for future consideration is a wing design with a lower aspect ratio. Finite element analysis of the current ultra-high AR wing shows noticeable wingtip deformation under extreme loading conditions. Though there is enough ground clearance and safety factor for stress, fatigue and dynamic flutters were not captured in the simulations. Theoretically, a shorter wingspan will be able to help with the following features: fatigue due to fluttering deformation, stress concentration at wing-fuselage junctions, maintenance cost, and design cost for innovative technology. For future improvements, we designed an alternative wing with AR at 9 with enlarged root chord and shortened wingspan. As shown in the 2g ramp bump FEA results, the stress and deformation were both reduced to a negligible level (Figure 13-1 & 13-2). This will likely help with structural rigidity and lifes-span and possibly save more weight due to a more compact design. Further mission-level analysis and higher fidelity CFD capturing dynamic aerodynamic perturbations are recommended to determine whether a higher or a lower aspect ratio is better.



**Fig. 13-1.** Von Mises stress for low AR wing design under 2g bump loading. The highest stress decreased to 825 psi compared to the 3050 psi in the current design.



**Fig. 13-2.** Wing flex deformation for low AR wing design under 2g bump loading. The tip drops 0.138 ft compared to the 1.413 ft in the current design.

The next improvement would be to redesign the landing gear configuration to better fit our design. For our aircraft we decided to use a pre-existing landing gear so we would not have to come up with a completely new design, allowing us to design our aircraft's fuselage to be compatible with whatever design we chose in the end. This worked to our team's advantage because after a critical design review, we realized that although our aircraft's engines would be just the right size, we would want to increase ground clearance as an extra safety precaution to protect the aircraft's engines from touching the ground surface on takeoff and/or landing. Our team is confident that

this ground clearance problem could be solved most effectively by configuring different landing gears in order to account for the extra needed clearance. We believe this is also the most cost and time effective solution because this change will allow us to keep our same overall aircraft design while in turn adding the needed clearance.

An additional improvement would be to modify and improve the current payload release system. Our payload system was originally designed to not only drop the needed payload from the aircraft, but to also serve as a system that could help stabilize the aircraft's center of gravity since this value would be constantly changing due to moving liquids onboard. Conversely, this payload system may cause problems down the road due to the added weight from the magnetic addition in order for this system to work properly. We have a few solutions in mind that could solve this problem, such as making the payload system out of a more lightweight material and keeping the rail system, but fixing the payload compartments in place.

## 14. Conclusion

Aerial firefighting is a key component of mitigating wildfires, and as global climate change continues to worsen, the need for this method is increasing. The current firefighting fleet consists mostly of outdated, repurposed airframes, so designing an aerial firefighting aircraft specifically to combat wildfires will increase operational efficiency. Material Girl alleviates capability gaps currently existing in the field by providing a new design that meets the requirements listed by the AIAA's RFP.

Through this design, the overarching goals that Material Girl attempted to optimize were maximum takeoff weight, fuel efficiency, control and maneuverability, and customizable payload deployment. Through these characteristics, our aircraft is a much more optimal choice in comparison to other designs in the field. The team maximized aerodynamic performance through the wing shape, optimizing sweep angle, aspect ratio, planform area, and airfoil choice. Along with this, large control surfaces – flaps, and flaperons – were added to the wings to enhance the maneuvering capabilities. By improving the aerodynamic capabilities of Material Girl through our selected configuration and parameters, the overall fuel burn and takeoff weight of the aircraft was lowered, which makes our aircraft sustainable. A unique payload deployment system was proposed that would be optional to the consumer, but provides benefits in maneuvering a large air tanker and supporting multiple mission profiles. A market analysis for the Material Girl was conducted, and while it is more expensive than current options, our design's longevity, sustainability and efficiency will let it outlast its competitors, making it a compelling alternative to the state of the art.

In conclusion, Material Girl tackles the challenge of larger fire containment through its robust, unique design. With high maneuverability, low stall speed options, and a modular payload deployment system, this aircraft is capable of achieving any mission profile requiring the objectives set forth in the RFP. In a future preliminary report, we look to further the Material Girl's development through use of detailed computational analysis and enhanced digital modeling.

## References

Beam, A. (2021, September 09). *California oks new spending on drought, wildfire prevention.*

<https://apnews.com/article/business-health-fires-climate-california-eec48e6279099449851b3c7f150cda33>

Boeing (2007). 757-200F (Page 13). Retrieved from:

[boeing.com/resources/boeingdotcom/company/about\\_bca/startup/pdf/freighters/757f.pdf](http://boeing.com/resources/boeingdotcom/company/about_bca/startup/pdf/freighters/757f.pdf)

Bonsor, K., & Chandler, N. (2019, May 20). How maglev trains work. HowStuffWorks.

<https://science.howstuffworks.com/transport/engines-equipment/maglev-train.htm>

Bradley, M. K., & Droney, C. K. (2015). Subsonic Ultra Green Aircraft Research: Phase II –

Volume II – Hybrid Electric Design Exploration (NASA/CR–2015-218704). National Aeronautics and Space Administration. <https://core.ac.uk/download/pdf/42706577.pdf>

Brandt, S. A., Stiles, R. J., Bertin, J. J., & Whitford, R. (2004). Introduction to Aeronautics: A

Design Perspective (2nd ed.). Reston, VA: American Institute of Aeronautics and Astronautics, Inc.

Dickenson, R. L. (1953). Aerodynamic data for structural loads (LR 9072). Lockheed.

<https://apps.dtic.mil/sti/pdfs/ADA953109.pdf>

Grover, H. J. (1966). Fatigue of aircraft structures. United States. Naval Air Systems

Command. <https://apps.dtic.mil/sti/pdfs/AD0660529.pdf>, Chapter XVII, p. 239-248

Hefley, R. K., & Jewell, W. F. (1972). Aircraft Handling Qualities Data (NASA CR-2144).

National Aeronautics and Space Administration. <https://www.robertheffley.com/docs/Data/NASA%20CR-2144--Hefley--Aircraft%20Handling%20Qualities%20Data.pdf>

Modern Airlines (2022). Boeing 737 Specifications. Retrieved from:

<https://modernairliners.com/boeing-737/boeing-737-specifications/>

Modern Airlines (2022). McDonnell Douglas DC-10, specs table. Retrieved from:



<https://modernairliners.com/mcdonnell-douglas-dc-10/>

Nicolai, L. M., & Carichner, G. E. (2010). Fundamentals of Aircraft and Airship Design: Volume

I - Aircraft Design. J. A. Schetz (Ed.). AIAA

Nelson, R. C. (1998). Flight Stability and Automatic Control (2nd ed.). WBC McGraw-Hill.

Pendrill, A. M., Karlsteen, M., & Rödjegård, H. (2012). Stopping a roller coaster train. IOP Science Physics

Education, 47(6), 728-735. <https://iopscience.iop.org/article/10.1088/0031-9120/47/6/728>

Raymer, D. P., (2018). Aircraft Design: A Conceptual Approach (6th ed.) AIAA Education

Series

Schauffle, R. D. (2007). The Elements of Aircraft Preliminary Design. Aries Publications.

The Learning Network. (2020, April 30). What's going on in this graph? | global temperature change.

<https://www.nytimes.com/2020/04/23/learning/whats-going-on-in-this-graph-global-temperature-change.html>

Wukovits, R., (2011) Popular calculator to calculate takeoff parameters in / from Airbus type | Rating: 5!.

<https://www.avsimrus.com/f/for-pilots-19/popular-calculator-to-calculate-takeoff-parameters-in-from-airbus-type-36340.html#file-36340>